

Efficient Few-Shot Continual Learning in Vision-Language Models

Aristeidis Panos¹ Rahaf Aljundi² Daniel Olmeda Reino² Richard E. Turner¹

Abstract

Vision-language models (VLMs) excel in tasks such as visual question answering and image captioning. However, VLMs are often limited by their use of pretrained image encoders, like CLIP, leading to image understanding errors that hinder overall performance. On top of that, real-world applications often require the model to be continuously adapted as new and often limited data continuously arrive. To address this, we propose LoRSU (Low-Rank Adaptation with Structured Updates), a robust and computationally efficient method for selectively updating image encoders within VLMs. LoRSU introduces structured and localized parameter updates, effectively correcting performance on previously error-prone data while preserving the model’s general robustness. Our approach leverages theoretical insights to identify and update only the most critical parameters, achieving significant resource efficiency. Specifically, we demonstrate that LoRSU reduces computational overhead by over 25x compared to full VLM updates, without sacrificing performance. Experimental results on VQA tasks in the few-shot continual learning setting, validate LoRSU’s scalability, efficiency, and effectiveness, making it a compelling solution for image encoder adaptation in resource-constrained environments.

1. Introduction

Large Language Models (LLMs) have revolutionized natural language understanding and generation, enabling significant advancements across diverse applications. As intelligent agents are increasingly expected to operate in real-world multimodal environments, integrating visual understanding becomes essential. Vision-Language Models (VLMs) extend LLMs by incorporating visual information, either through pre-trained vision encoders or end-to-end multimodal training. These models have demonstrated state-of-

¹University of Cambridge ²Toyota Motor Europe. Correspondence to: Aristeidis Panos <ap2313@cam.ac.uk>.

the-art performance on vision-language tasks such as visual question answering (VQA) and image captioning, highlighting their potential for general-purpose multimodal reasoning (Chen et al., 2024; Wang et al., 2024a).

Approaches that rely on pretrained image encoders typically use variants of the CLIP model (Radford et al., 2021), which is kept frozen in the vision-language binding process (Liu et al., 2024b). CLIP is a widely deployed vision transformer that has strong zero-shot capabilities in various tasks and domains. However several existing works have highlighted various weaknesses of CLIP on out of domain data (Liu et al., 2024b; Zhu et al., 2023; Chen et al., 2023; Li et al., 2023; Tong et al., 2024). When deploying VLMs as visual assistants in new domains, it is then expected that VLMs can be updated using a few images gathered from the target environment whenever deficiencies are noted.

Continual learning allows a model to be continuously updated as new data from new tasks or domains are encountered. Recent literature on continual learning (CL) of vision language models focus on updating either the LLM (Srivastava et al., 2024) or language projection layers (Das et al., 2024), maintaining a frozen image encoder.

In vision language models, the LLM component provides reasoning and factual knowledge, while the image encoder’s role is to extract robust and accurate visual features. In this work, we argue that adapting VLMs to new visual domains or tasks is more effective and efficient when the image encoder is updated rather than the LLM. Figure 1 highlights this issue using images from the Toyota Smart Home dataset (TSI) (Das et al., 2019) dataset: in the first column, LLaVA (Liu et al., 2024a) struggles to recognize the person’s action in the original image but accurately describes the same action in a generated image from OpenAI’s DALL·E 2. This example underscores that the visual shift, rather than the LLM’s understanding of the action, is the main source of weakness.

Motivated by the above limitations, we introduce a novel parameter-efficient fine-tuning (PEFT) method called LoRSU (Low-Rank Adaptation with Structured Updates) for selectively updating specific modules of the transformer blocks of image encoders within VLMs. The right column of Figure 1 illustrates the (correct) responses of LLaVA after updating the image encoder separately with our method on

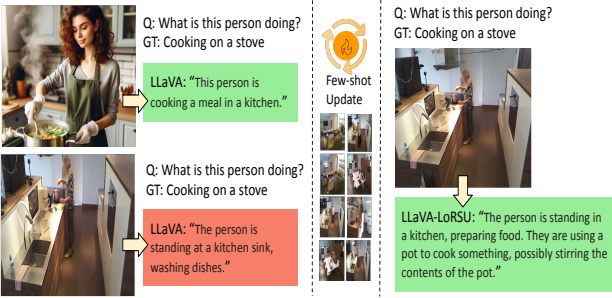


Figure 1. (Left) Responses of the pretrained LLaVA to samples from TSI dataset (bottom) compared to DALL-E 2 generated images (top) for the ‘cooking on a stove’ class. (Right) LLaVA’s correct response to the same TSI image after fine-tuning LLaVA using LoRSU.

a low-number of samples from TSI dataset compared to the pretrained LLaVA’s (wrong) response.

Through extensive experiments, we demonstrate that updating the image encoder is essential for improving the performance of the VLM that relies on it. More importantly, this approach is computationally efficient, as the image encoder has significantly fewer parameters compared to the language model and the method is less prone to forgetting, especially the LLM knowledge.

We evaluated our approach on various VQA tasks comparing to state-of-the-art CL methods and the PEFT baseline LoRA(Hu et al., 2021) on various few-shot CL settings. We show significant improvements of the full VLM model on all settings and very low rates of forgetting without using any replay buffer of data from the previous tasks. By selectively updating the image encoder, our method provides a robust and efficient solution for handling visual shifts. This targeted adaptation strategy avoids the need to modify the entire model, preserving existing knowledge whilst ensuring strong performance in new domains.

The contributions of the paper are as follows:

- We propose LoRSU, a novel replay-free PEFT method tailored for few-shot continual learning.
- We introduce two new VQA datasets, TSI and DALLE, created to expose the limitations of pre-trained image encoders in VLMs.
- We conduct the first large-scale study of few-shot CL in VLMs, evaluating LoRSU across ten diverse VQA datasets and benchmarking against state-of-the-art PEFT and CL methods. LoRSU consistently outperforms all baselines.

2. Related Work

Continual Learning. Our work falls within the continual learning literature, where a model needs to be updated incrementally as new data arrive, accumulating knowledge over tasks and reducing forgetting of previously acquired information (De Lange et al., 2021).

Continual Learning for Multimodal Language Models. Wu et al. (2024) provide a survey on continual learning for LLMs, highlighting challenges of computational efficiency and forgetting. Srivastava et al. (2024) explored continual multi-modal learning on VQA datasets, keeping the vision encoder frozen. He et al. (2023b) examined continual instruction tuning with sequential VQA datasets, proposing a method where the projection head is expanded for each new task. Das et al. (2024) introduced a pseudo-rehearsal strategy for vision-language models, updating only the language projection layer. Our method adapts only the vision encoder, preserving language capabilities.

Continual Learning with Few-Shot Updates. Verwimp et al. (2023) posits that an ideal continual learning solution would enable continual correction of model’s mistakes at a lower computational cost than retraining from scratch. However, most continual few-shot learning from pre-trained models focuses on classification tasks and introduces solutions that cannot scale to large multimodal models. Panos et al. (2023) update the vision encoder on the first task only, later adapting a covariance matrix for incoming tasks. Goswami et al. (2024) calibrate the covariance matrix for new classes based on semantic similarity. Zhao et al. (2024) introduce few and slow updates, proposing a transfer loss function and a cross-classification loss to mitigate catastrophic forgetting. Few-shot updates can also be viewed through the lens of model editing (Sinitin et al., 2020). MEND (Mitchell et al., 2022) scales model editing to large language models by transforming the gradient obtained from fine-tuning, through a low-rank decomposition fed to auxiliary networks designed to make fast, local edits to a pre-trained model, requiring a set of unrelated examples to prevent forgetting. ROME (Meng et al., 2022) applies causal tracing to identify layers where incorrect factual knowledge is stored, applying a low-rank update. However, ROME does not scale to continual updates or non-association types of updates. Cheng et al. (2023) studied multi-modal editing, showing negligible deterioration in multi-modal task performance when updating language models but severe forgetting when updating vision encoders. To the contrary, our method focuses on adapting the vision encoder rather than updating the factual knowledge in the LLM, yet achieving strong performance gains and negligible forgetting.

Continual Learning of Pre-Trained Image Encoders. SPT (He et al., 2023a) estimates a mask of updates based on parameter sensitivity, performing low-rank or

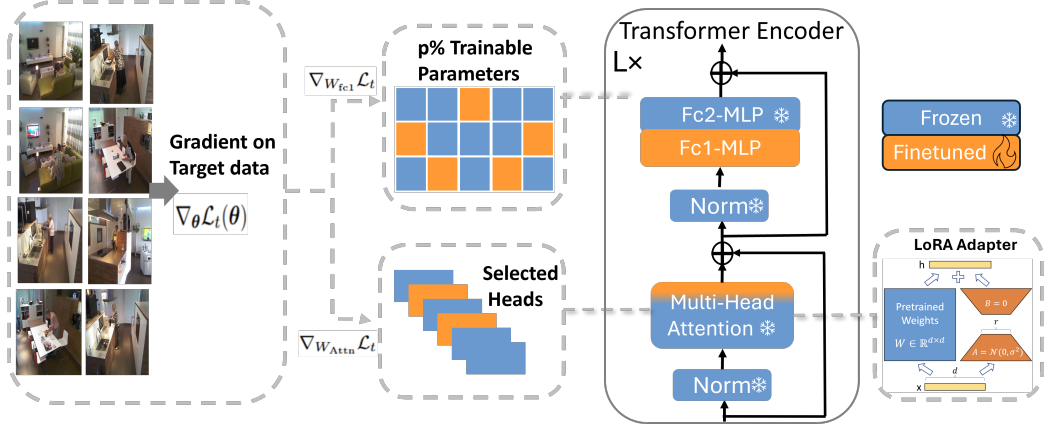


Figure 2. LoRSU mechanism: After computing the gradient $\nabla_{\theta} \mathcal{L}_t(\theta)$ over the target dataset at time t , LoRSU picks a small number of attention heads and a small number of parameters from the first linear layer of the MLP module in the transformer block based on the magnitude of the gradients of $\nabla_{W_{\text{Attn}}} \mathcal{L}_t$ and $\nabla_{W_{\text{fc1}}} \mathcal{L}_t$, respectively. Computational efficiency is ensured by introducing LoRA adapters to the attention weight matrices.

sparse updates. SPU (Zhang et al., 2024) localizes updates to the first feed-forward layer of each transformer block, inspired by knowledge neuron theory (Dai et al., 2021). Our approach generalizes updates to all layers, selecting relevant parameters and maintaining gradient norms, combined with LoRA on selected attention heads for adaptivity and stability, achieving SOTA performance on continual fewshot multimodal tasks.

3. Low-Rank Adaptation with Structured Updates

Few-shot continual learning is a highly practical and challenging scenario, where models must incrementally adapt to new tasks with limited supervision while retaining previously acquired knowledge. This setting closely mirrors real-world applications, such as interactive AI assistants and autonomous systems, where models receive a continuous stream of novel data but only sparse supervision per update.

To address the challenge of efficiently fine-tuning large-scale visual encoders and transformer-based models under the few-shot continual learning setting, without causing catastrophic forgetting (i.e., degradation in performance on previously learned tasks), we propose a novel parameter-efficient fine-tuning method called *Low-Rank Adaptation with Structured Updates* (**LoRSU**).

LoRSU updates specific parameters within each transformer block in a resource-efficient manner, mitigating the risk of generic knowledge loss when fine-tuning for new tasks. Specifically, we selectively update a subset of parameters from the first linear layer in the MLP block of each transformer layer, as proposed in (Zhang et al., 2024). While this approach reduces the fine-tuning burden, it may limit model

flexibility as the remaining parameters in the transformer block remain fixed. To enhance flexibility, we further update the most informative attention heads based on the gradient of the task-specific loss.

More specifically, let a dataset $\mathcal{D}_t = \{\mathbf{x}_n, \mathbf{y}_n\}_{n=1}^{N_t}$ for the current task t where \mathbf{x}_n is an image with text description \mathbf{y}_n . We define $\mathcal{L}(\theta; \mathcal{D}_t) := \mathcal{L}_t(\theta)$ as the loss used for training the model and $\theta \in \mathbb{R}^d$ is the full set of model's parameters. The standard Multi-head Self-Attention Mechanism (MSA) (Vaswani et al., 2017), comprised of H D_h -dimensional heads, is defined as the concatenation of multiple self-attention (SA) blocks where $\mathbf{q}^{(i)} = W_q^{(i)} Z^\top, \mathbf{k}^{(i)} = W_k^{(i)} Z^\top, \mathbf{v}^{(i)} = W_v^{(i)} Z^\top \in \mathbb{R}^{D_h \times N}$, are the query, key and value matrices, which are used to compute the self-attention outputs as follows

$$A^{(i)} = \text{softmax}(\mathbf{q}^{(i)\top} \mathbf{k}^{(i)} / \sqrt{D_h}) \in \mathbb{R}^{N \times N}, \quad (1)$$

$$\text{SA}_i(Z) = A^{(i)} \mathbf{v}^{(i)\top} \in \mathbb{R}^{N \times D_h}, \quad i = 1, \dots, H. \quad (2)$$

$Z \in \mathbb{R}^{N \times D}$ is the input matrix of N tokens of dimension D and $W_q^{(i)}, W_k^{(i)}$, and $W_v^{(i)}$ are the query, key, and value matrices of learnable parameters for head i , respectively. The final MSA function is defined as $\text{MSA}(Z) = \text{Concat}[\text{SA}_1(Z), \dots, \text{SA}_H(Z)] W_o \in \mathbb{R}^{N \times D}$, $W_o \in \mathbb{R}^{HD_h \times D}$.

Since we care to update the parameters of the heads that cause the largest changes in $\mathcal{L}_t(\theta)$, we compute the gradient of the loss with respect to the parameters of each head and then we update only those heads with the largest cumulative contribution to the loss change. Since the matrices $W_q^{(i)}, W_k^{(i)}, W_v^{(i)}$ are all the parameters of head i , we can define an importance score for each head by adding the squared values of their corresponding gradients $G_q^{(i)} = \nabla_{W_q^{(i)}} \mathcal{L}_t$,

$G_k^{(i)} = \nabla_{W_k^{(i)}} \mathcal{L}_t$, and $G_v^{(i)} = \nabla_{W_v^{(i)}} \mathcal{L}_t$, as follows

$$s_i = \sum_{m,l} \left((G_q^{(i)}[m,l])^2 + (G_k^{(i)}[m,l])^2 + (G_v^{(i)}[m,l])^2 \right). \quad (3)$$

We provide a theoretical justification of (3) in the next section. We update only the top- k heads, based on their importance scores $\{s_1, \dots, s_H\}$, $I \subset \{1, \dots, H\}$, to be updated on the current task. Nevertheless, the number of parameters remain high due to the large weight matrices. Therefore, we parametrize the original weights using LoRA (Hu et al., 2021) to further reduce the computational burden. The matrices $W_q^{(i)}, W_k^{(i)}, W_v^{(i)}, i \in I$ are now defined as

$$W_\alpha^{(i)'} = W_\alpha^{(i)} + A_\alpha^{(i)} B_\alpha^{(i)}, \quad \alpha \in \{q, k, v\}. \quad (4)$$

Finally, to ensure that we only update $W_q^{(i)}, W_k^{(i)}, W_v^{(i)}, \forall i \in I$ we use a binary mask on the gradient vector with respect to all parameters of all attention heads. We keep the projection matrix W_o frozen. We note that most modern implementations of transformer blocks concatenate the three attention weight matrices W_q, W_k, W_v into one and thus we only need to apply LoRA once to this concatenated matrix.

Regarding the first linear layer in the MLP module, $W_{\text{fc}1} \in \mathbb{R}^{d \times D}$, we mask the gradients of $W_{\text{fc}1}$ so only the most important parameters for the current task to be updated, i.e. we use the following biased gradient update.

$$\hat{\nabla}_{W_{\text{fc}1}} \mathcal{L}_t = M_{\text{fc}1} \odot \nabla_{W_{\text{fc}1}} \mathcal{L}_t, \quad (5)$$

where $M_{\text{fc}1} \in \{0, 1\}^{d \times D}$ is a zero-one mask that is built by choosing a proportion of the largest squared values of $\nabla_{W_{\text{fc}1}} \mathcal{L}_t$ in a similar manner as in (Zhang et al., 2024) and \odot is the Hadamard product.

Theoretical justification. The importance scores in (3) can be derived from the following constrained (binary) optimization problem¹

$$\begin{aligned} \mathbf{p}^* &= \arg \max_{\mathbf{p} \in \{0,1\}^d} \frac{\|\mathbf{p} \odot \nabla_W \mathcal{L}(\boldsymbol{\theta}_0)\|^2}{\|\nabla_W \mathcal{L}(\boldsymbol{\theta}_0)\|^2}, \\ \text{s.t. } &\bigcup_{\ell=1}^G I_\ell \subset \{1, 2, \dots, d\}, \quad I_i \cap I_j = \emptyset, \quad \forall i \neq j, \\ \text{and } &C = \sum_{\ell=1}^G c_\ell, \quad c_\ell \leq |I_\ell| \quad \forall \ell, \quad \|\mathbf{p}\|_0 \leq C, \end{aligned} \quad (6)$$

where $\boldsymbol{\theta}_0$ is the vector of the pretrained parameters before using \mathcal{D}_t for fine-tuning the model. The groups of parameters I_i correspond to the parameters of a specific module (e.g.

¹For notational simplicity, we assume a single transformer block for this case.

Self-Attention or MLP projector) we aim to learn, hence the constraint of mutually exclusiveness, $I_i \cap I_j = \emptyset$, between different pairs of parameter groups. Also note that we allowed to choose a subset c_ℓ of the parameters of a specific group I_ℓ which is the underneath mechanism of LoRSU choosing attention heads and parameters of fc1. The mask \mathbf{p}^* is chosen so that the gradient norm of the masked gradients is as large as possible under the sparsity constraints. We prove in appendix A that the indices of the non-zero values of \mathbf{p}^* can be found using the importance scores in (3) and the magnitudes of the gradients with respect to the fc1 parameters.

4. Experiments

We conduct a series of experiments under three different few-shot continual learning (CL) settings (CL-5, CL-20, and CL-50 shots) to thoroughly investigate the performance of LoRSU based on ten VQA datasets. By adopting this paradigm, we aim to assess the adaptability and efficiency of LoRSU under constrained learning conditions, ensuring that it remains both computationally feasible and effective in improving downstream performance. Specifically, we seek to address the following key questions: 1) How does our method, LoRSU, compare to other fine-tuning and CL baselines that use the CLIP loss to update the image encoder? 2) Does updating the image encoder separately and then reintegrating it into the corresponding VLM enhance downstream VQA performance? 3) What is the effect of using the perplexity loss instead of the CLIP loss to update the image encoder? 4) What are the benefits of choosing a subset of attention heads to be fine-tuned using LoRSU? and 5) What are the computational benefits of LoRSU?

4.1. Datasets

We evaluate the performance of LoRSU on ten visual question answering (VQA) datasets falling in two broad categories: regular VQA datasets and classification datasets converted to VQA datasets.

Regular VQA datasets. We consider four standard VQA datasets used for benchmarking VLMs' performance (Duan et al., 2024): *VSR* (Liu et al., 2023), the Visual Spatial Reasoning corpus consists of caption-image pairs labeled as True or False, where each caption describes the spatial relation between two objects in the image. VLMs evaluate whether the caption accurately reflects the image. *HM* (Kielia et al., 2020), the Hateful Memes dataset designed to detect multimodal hateful memes. *MMVP* (Tong et al., 2024), the Multimodal Visual Patterns dataset is a challenging benchmark which has been built on images that CLIP perceives as similar despite their clear visual differences. *VisOnly* (Kamoi et al., 2024), a novel dataset created to directly assess the visual perception abilities of VLMs in

answering questions about geometric and numerical details in scientific figures. This dataset allows us to assess fine-grained visual perception in VLMs independently of other abilities, such as reasoning, making it the most challenging among the previously mentioned datasets.

Classification-to-VQA datasets. We convert four popular multi-class classification datasets into multiple-choice VQA problems, where each question has five choices, and the VLM is tasked with selecting the correct answer. These datasets are introduced as examples of scenarios where visual domain shifts are encountered, allowing us to examine the utility of updating the image encoder; a critical consideration often overlooked in many standard VQA datasets. The datasets include: *GTS* (Stallkamp et al., 2012), the German Traffic Sign dataset, which Zhang et al. (2024) considered as an out-of-distribution dataset for CLIP pre-training; *CAn* (Wang et al., 2024b), a recent dataset created to test CLIP’s robustness with animal images containing realistic spurious features such as unexpected backgrounds; *AIR* (Maji et al., 2013), a fine-grained aircraft classification dataset; *ESAT* (Helber et al., 2019), a dataset of satellite images used for land cover classification.

TSI & DALLE. In addition to these existing datasets, we introduce two novel VQA datasets: TSI and DALLE, both designed to explore the effects of domain shift. The *TSI* (Das et al., 2019) dataset was preprocessed as a classification dataset, where the goal is to recognize the activity depicted in each image. Frames were extracted from videos to create a training set of approximately 10K images and a test set of approximately 5K images, encompassing 27 distinct activity classes. The *DALLE* dataset, constructed by querying the OpenAI’s model DALL-E 2, includes representative images generated from 22 activity classes appearing in TSI. For each activity, we generated 30 images, resulting in a total of 660 images designated exclusively for evaluation purposes.

We follow the common practice in few-shot continual learning (Panos et al., 2023) to construct the sequences. We divide each dataset into 5 sets of disjoint classes/categories and consider 5/20/50 shot settings where only 5/20/50 images per class in the current set are used for fine-tuning the model. More details on how we split each of these datasets for the CL settings are provided in appendix C.

4.2. Experimental Setting

Metrics. While standard metrics in the CL literature exist to evaluate general performance (Lopez-Paz & Ranzato, 2017; Chaudhry et al., 2018), VLMs exhibit generic knowledge across various domains beyond the one being adapted, making it crucial to evaluate how adaptation impacts their overall performance. These metrics do not measure the change in performance relative to the model’s initial state prior to the learning process. To address this, we use the

zero-shot accuracy of each VQA dataset as the benchmark baseline and report the change in accuracy on the test split of the target dataset so positive values indicate an improvement in accuracy. This approach enables us to quantify the model’s ability to accumulate knowledge, using the pre-trained model as the reference point; we name this metric as *Target Improvement* (TI) accuracy. We also calculate the average accuracy change on the test splits of the remaining datasets, when fine-tuning on a specific dataset, to estimate average forgetting of generic knowledge or possible positive backward transfer (De Lange et al., 2021); we call this metric *Control Change* (CC) accuracy where ‘control’ refers to the control datasets we use to calculate the average accuracy change. TI and CC are computed based on the fine-tuned VLM after the last session of CL. We also consider standard CL performance metrics such as *Average Accuracy* (ACC) and *Backward Transfer* (BWT) (Lopez-Paz & Ranzato, 2017) to examine how accuracy and forgetting evolves through continuous adaptation. Notice that these metrics, in contrast to TI and CC, focus on the accuracy and forgetting during continual adaptation and they do not take into account the performance of the fine-tuned model on other datasets.

Implementation details. Please see Appendix B.

Models. For our experiments, we consider the popular Vision Language Model LLaVA-v1.5 (Liu et al., 2024b) that leverages a frozen CLIP image encoder. Specifically, LLaVA utilizes a frozen OpenAI-CLIP-L-14 (Radford et al., 2021) with a LLM (Vicuna-7b (Chiang et al., 2023)). The two modules are connected through a two-layer MLP projector that aligns image and text features. The LLM and the MLP projector are optimized during the visual instruction tuning while CLIP remains frozen. LLaVA concatenates adjacent tokens from CLIP-L-14 and processes them with an MLP projector as input to LLama-2 (7B-chat) (Touvron et al., 2023); the MLP projector and the language model are optimized while the image encoder remains frozen.

Baselines. We compare LoRSU to the following methods that also use the CLIP loss to fine-tune the image encoder:

- *LN* (Perez et al., 2018; Panos et al., 2023) is used for both few-shot and CL. Only the image encoder LayerNorm modules’ parameters are optimized.
- *F-FT* is the standard fine-tuning technique where all image encoder parameters undergo gradient updates.
- *F-EWC* fine-tunes all the image encoder parameters with EWC regularization (Kirkpatrick et al., 2017).
- *LoRA* (Hu et al., 2021) a popular PEFT method which parameterizes incremental updates by two low-dimensional matrices and only fine-tunes them.
- *AdaLoRA* (Zhang et al., 2023) dynamically adjusts the low-rank update budget allocation during training.

Table 1. Performance comparison of LoRSU with the CLIP loss against baselines fine-tuning the image encoder using the same loss. We report the *Target Improvement* (TI) and *Control Change* (CC) accuracies across three different continual learning (CL) settings. Greener shades indicate higher positive values, while redder shades signify lower negative values. The highest accuracies across methods for each dataset are underlined.

Setting	FT Dataset	FT Method													
		LN		F-FT		F-EWC		LoRA		AdaLoRA		SPU		LoRSU	
		TI (\uparrow)	CC (\uparrow)	TI (\uparrow)	CC (\uparrow)	TI (\uparrow)	CC (\uparrow)	TI (\uparrow)	CC (\uparrow)	TI (\uparrow)	CC (\uparrow)	TI (\uparrow)	CC (\uparrow)	TI (\uparrow)	CC (\uparrow)
CL-5	GTS	3.5	-1.5	3.7	-6.5	5.0	-11.5	0.7	-4.8	-0.9	-4.9	5.4	-0.6	6.4	-0.7
	TSI	0.8	0.0	7.4	-1.1	8.5	-1.0	-0.1	-2.8	1.1	0.2	0.9	0.1	3.2	0.1
	CAn	-2.4	-0.2	-2.4	-2.2	-16.7	-9.4	-1.3	-4.6	-1.0	-0.1	-0.4	0.1	0.3	0.3
	AIR	0.3	-1.6	2.0	-2.7	2.9	-2.8	1.3	-3.7	0.4	0.0	3.1	0.1	4.8	0.4
	ESAT	4.2	0.6	-10.3	-1.4	-8.4	-2.1	-1.6	-0.7	1.9	0.1	4.5	0.1	6.8	0.2
CL-20	GTS	5.2	-5.9	4.6	-7.3	6.7	-15.6	2.5	-10.5	0.2	-2.2	7.9	-1.3	8.6	-1.0
	TSI	5.1	-1.9	15.3	-3.4	16.0	-32.5	8.5	-4.4	1.3	-9.6	7.8	-0.3	10.6	-0.1
	CAn	-2.4	-0.4	0.3	-2.9	0.1	-5.1	-2.3	-5.4	-3.5	-2.5	0.1	0.5	1.1	0.3
	AIR	-0.2	-3.0	9.3	-1.8	10.2	-2.0	5.3	-2.7	2.7	-0.7	3.0	-0.2	5.9	-0.5
	ESAT	0.9	-0.1	-24.9	-1.7	-22.0	-3.8	-11.5	-0.5	-6.8	-2.7	5.4	0.3	6.6	0.2
CL-50	GTS	4.8	-6.5	3.4	-9.8	5.3	-12.9	3.1	-11.1	1.0	-3.3	7.7	-1.5	9.7	-1.3
	TSI	7.0	-3.0	17.2	-4.6	22.4	-13.4	18.2	-6.3	7.9	-1.9	12.2	-0.5	19.1	-0.3
	CAn	-5.7	-3.3	-1.0	-4.9	0.6	-9.7	-0.4	-4.4	-1.8	-0.8	0.6	-0.3	1.3	-0.5
	AIR	1.8	-3.9	10.0	-3.1	10.9	-3.3	7.8	-3.8	4.6	-0.9	6.2	-0.6	8.2	-0.7
	ESAT	4.6	0.1	-41.4	-3.3	-38.1	-2.0	-14.5	-3.6	-17.3	-2.4	5.8	0.1	7.0	0.2

- *SPU* (Zhang et al., 2024) is a PEFT baseline, specifically designed to tackle catastrophic forgetting in CL scenarios, that utilizes structured sparsity based on gradient information to fine-tune the most significant parameters of the fc1 module in the transformer block.

4.3. CLIP-based Updates

We evaluate the performance of the Vision-Language Model (VLM) when only the image encoder is fine-tuned using the CLIP loss in a CL setting. This experiment compares six strong CLIP-based baselines with our proposed method, LoRSU. Table 1 reports the average accuracies of TI/CC over three runs; detailed results can be found in appendix D. We observe that LoRSU consistently achieves superior TI scores across datasets and CL settings, underscoring its ability to enhance task-specific performance effectively. Furthermore, LoRSU maintains CC accuracies that take consistently small negative or even positive values, highlighting its capacity to preserve or slightly improve performance on control datasets while fine-tuning on target datasets. Even in datasets where other methods struggle (e.g., CAn, ESAT), LoRSU often performs better, maintaining positive or close-to-neutral TI and CC scores. For instance, In ESAT (CL-50) containing challenging satellite images, LoRSU achieves

Table 2. Average accuracy (ACC) (\uparrow) and backward transfer (BWT) (\uparrow) scores (%). For reference, the ACC of the pretrained model on GTS and ESAT is 75.4 and 76.4, respectively, while BWT is zero for all cases. The highest scores across methods are underlined.

Setting	FT Dataset	LoRA		SPU		LoRSU	
		ACC	BWT	ACC	BWT	ACC	BWT
CL-5	GTS	79.2	-7.1	80.8	0.5	81.1	0.4
	ESAT	73.8	-3.4	79.8	1.5	82.2	2.0
CL-20	GTS	77.2	-9.1	82.8	-0.6	83.5	-0.4
	ESAT	64.1	-18.3	82.0	2.0	82.7	0.1
CL-50	GTS	79.3	-10.3	83.8	-0.7	84.7	-0.5
	ESAT	61.4	-27.8	81.2	-2.4	82.1	-0.8

the highest TI (7.0) with a positive CC (0.2), outperforming SPU (TI=5.8, CC=0.1) and all other methods.

Additional metrics. We assess the performance of LoRSU against LoRA and SPU in terms of ACC and BWT across two out-of-domain datasets, GTS and ESAT. Since LoRA and SPU have similar number of trainable parameters as LoRSU and competitive performance in our previous ex-

Table 3. Performance comparison between LoRSU using the CLIP loss (*LoRSU*) or the perplexity loss (*LoRSU-Ppl*) and other baselines that fine-tune only the vision encoder (*LoRA*, *LoRA-Ppl*), only the LLM (*LoRA-L*), or both of them (*LoRA-F*). We report the *Target Improvement* (TI) and *Control Change* (CC) for each CL setting. \dagger and \ddagger denote classification-to-VQA and regular VQA datasets, respectively. The highest accuracies across methods for each dataset are underlined.

Setting	FT Dataset	FT Method											
		LoRA-L		LoRA		LoRSU		LoRA-Ppl		LoRA-F		LoRSU-Ppl	
		TI (\uparrow)	CC (\uparrow)	TI (\uparrow)	CC (\uparrow)	TI (\uparrow)	CC (\uparrow)	TI (\uparrow)	CC (\uparrow)	TI (\uparrow)	CC (\uparrow)	TI (\uparrow)	CC (\uparrow)
CL-5	GTS †	-4.1	<u>-0.2</u>	0.7	-4.8	<u>6.4</u>	-0.7	-7.5	-3.0	-2.7	-1.8	1.6	-1.0
	TSI †	<u>6.0</u>	-0.1	-0.1	-2.8	3.2	0.1	<u>10.9</u>	-2.4	-8.0	-2.4	<u>13.1</u>	<u>1.5</u>
	CAN †	-3.3	-0.2	-1.3	-4.6	<u>0.3</u>	<u>0.3</u>	-3.5	-5.5	-4.1	-1.6	0.2	-0.2
	AIR †	-1.7	<u>0.3</u>	1.3	-3.7	4.8	<u>0.4</u>	-0.7	-1.5	<u>9.6</u>	-1.9	<u>5.8</u>	-0.2
	ESAT †	-0.2	-0.1	-1.6	-0.7	<u>6.8</u>	0.2	-0.6	<u>0.4</u>	5.4	-0.5	3.7	0.1
	VSR ‡	<u>16.8</u>	-0.6	0.5	-4.0	0.4	<u>0.2</u>	10.2	-12.5	<u>18.0</u>	-10.6	<u>10.5</u>	-1.2
	HM ‡	<u>7.4</u>	-2.7	-0.4	-6.8	0.6	<u>0.4</u>	-1.2	-1.2	6.0	-4.5	-0.8	0.2
	VisOnly ‡	-0.4	-0.1	-1.1	-4.5	0.9	0.1	0.3	-0.3	0.2	-0.4	<u>2.7</u>	<u>0.7</u>
CL-20	GTS †	-1.4	<u>0.1</u>	2.5	-10.5	<u>8.6</u>	-1.0	-0.5	-6.4	-1.4	-0.8	3.9	-0.7
	TSI †	<u>5.9</u>	<u>0.0</u>	<u>8.5</u>	-4.4	<u>10.6</u>	-0.1	<u>6.5</u>	-11.6	2.9	-3.1	<u>13.9</u>	-0.6
	CAN †	-1.9	-0.6	-2.3	-5.4	<u>1.1</u>	<u>0.3</u>	-3.7	-8.8	-2.1	-1.7	0.5	-1.2
	AIR †	3.7	<u>0.3</u>	<u>5.3</u>	-2.7	<u>5.9</u>	-0.5	4.8	-3.5	<u>16.3</u>	-0.3	<u>6.0</u>	-0.3
	ESAT †	0.7	<u>0.4</u>	-11.5	-0.5	<u>6.6</u>	0.2	-1.2	-0.1	-4.6	-0.0	2.9	-0.1
	VSR ‡	<u>22.2</u>	<u>1.0</u>	0.4	-3.9	0.1	-0.2	<u>19.5</u>	-0.3	<u>23.3</u>	-5.1	<u>22.9</u>	-1.6
	HM ‡	<u>10.6</u>	-2.2	-1.8	-5.8	0.7	<u>0.2</u>	<u>10.7</u>	-0.1	<u>11.7</u>	-1.4	<u>10.9</u>	-0.2
	VisOnly ‡	-2.3	<u>0.7</u>	-1.0	-4.7	0.2	0.1	-2.0	<u>0.5</u>	-1.0	0.2	<u>1.7</u>	<u>0.5</u>
CL-50	GTS †	-0.7	<u>-0.3</u>	3.1	-11.1	<u>9.7</u>	-1.3	-1.4	-6.7	-3.9	-2.1	6.9	-0.4
	TSI †	<u>9.9</u>	<u>-0.0</u>	18.2	-6.3	<u>19.1</u>	-0.4	-1.6	-16.5	<u>15.1</u>	-0.7	<u>22.0</u>	-1.1
	CAN †	-1.8	-0.7	-0.4	-4.4	<u>1.3</u>	<u>-0.5</u>	-1.8	-9.8	-2.1	-1.1	1.0	-3.4
	AIR †	4.6	<u>0.4</u>	<u>7.8</u>	-3.8	<u>8.2</u>	-0.7	6.2	-3.1	<u>17.9</u>	-0.9	<u>8.9</u>	-0.4
	ESAT †	1.0	<u>0.2</u>	-14.5	-3.6	<u>7.0</u>	0.2	1.7	0.2	-9.5	-0.6	-0.7	-0.5
	VSR ‡	<u>21.9</u>	<u>1.0</u>	0.4	-4.5	2.3	-0.3	<u>20.2</u>	-5.3	<u>21.0</u>	<u>1.1</u>	<u>23.4</u>	-3.6
	HM ‡	<u>10.2</u>	-2.1	0.7	-4.5	0.3	<u>0.2</u>	<u>12.5</u>	-1.5	<u>12.3</u>	-3.7	<u>12.2</u>	<u>0.2</u>
	VisOnly ‡	-2.4	<u>0.6</u>	-0.2	-6.8	0.3	-0.1	-2.0	<u>0.7</u>	0.2	0.2	<u>0.3</u>	0.1

periment, we choose those for comparison. Table 2 shows that LoRSU’s performs well with respect to these metrics, following similar patterns as TI and CC in Table 1. LoRSU achieves the best performance on ACC while exhibiting minimal forgetting with the least negative BWT values. Similar patterns are observed on extra datasets in appendix D.2.

4.4. CLIP-based vs. Perplexity-based Updates

Traditionally, LLMs and VLMs achieve impressive performance through fine-tuning with the perplexity loss. LoRA is the standard PEFT method for this purpose, and thus, we consider three extra LoRA variants plus *LoRSU-Ppl* which all utilize the perplexity loss to update the model.

- *LoRA-L* applies LoRA adapters to all weight matrices of the LLM and thus perplexity loss is required.
- *LoRA-Ppl* is the same method as LoRA but this time the perplexity loss is used to update the adapters.
- *LoRA-F* applies LoRA adapters to all weight matrices of the LLM, the image encoder, and the MLP projector.

We evaluate how LoRSU and LoRA perform compared to their perplexity-based counterparts, LoRSU-Ppl and LoRA-Ppl, respectively. Furthermore, we seek to explore how these methods compare to parameter-efficient fine-tuning approaches when either the entire VLM (LoRA-F) or only the LLM component (LoRA-L) is updated.

The results in Table 3 highlight the strong and robust per-

Table 4. Comparison of the importance of choosing a small subset of attention heads. The GTS dataset is used for fine-tuning. We include error bars over 3 runs. The highest accuracies across methods are underlined.

Setting	Scores	LoRSU-Rand	LoRSU-AAH	LoRSU
CL-5	TI (↑)	4.1 ± 0.4	5.9 ± 0.8	<u>6.4 ± 1.3</u>
	CC (↑)	-1.0 ± 0.5	-0.9 ± 0.3	<u>-0.7 ± 0.6</u>
CL-20	TI (↑)	6.2 ± 0.6	7.5 ± 0.6	<u>8.6 ± 0.9</u>
	CC (↑)	-1.4 ± 0.3	<u>-0.7 ± 0.4</u>	-1.0 ± 0.5
CL-50	TI (↑)	7.8 ± 0.4	9.1 ± 0.1	<u>9.7 ± 0.1</u>
	CC (↑)	-1.7 ± 0.2	<u>-0.9 ± 0.2</u>	-1.3 ± 0.1

formance of LoRSU and LoRSU-Ppl compared to other baseline methods across various settings. Both LoRSU and LoRSU-Ppl achieve minimal negative or even positive changes in CC, indicating reduced catastrophic forgetting and improved retention of generic knowledge compared to baselines. The table reports the average accuracies of TI/CC over three runs with exact results provided in appendix D.

The use of the perplexity loss in LoRSU-Ppl demonstrates a considerable improvement in TI accuracy over LoRSU when fine-tuned for VQA datasets. For instance, LoRSU-Ppl achieves 10% higher TI accuracy than LoRSU on VSR. We hypothesize that the perplexity loss acts as an additional signal that optimizes the image encoder to complement the frozen language model more effectively, improving the alignment between visual and textual modalities in VQA.

However, we observe that LoRSU achieves a balance between task-specific improvements and generalization, consistently demonstrating higher CC accuracy compared to LoRSU-Ppl across most datasets. Lastly, although LoRA-F achieves high TI scores on many datasets, it suffers significantly from forgetting, underscoring the importance of LoRSU’s structured updates in CL scenarios.

4.5. The Choice of Attention Heads

Given that LoRSU’s mechanism of choosing attention heads is a key-point to its success, we conduct an ablation study on the different strategies for selecting attention heads during the fine-tuning process. In this experiment, we compare LoRSU’s performance to two new variants of LoRSU, namely, *LoRSU-Rand* and *LoRSU-AAH*. LoRSU-Rand randomly chooses the number of attention heads ($k = 2$ heads) to be fine-tuned while LoRSU-AAH fine-tunes all the available attention heads (16 in total) in each transformer block. For extra results on the sensitivity of the number of LoRSU’s optimal attention heads k , see appendix E.2.

The results in Table 4 demonstrate that LoRSU’s targeted approach is performant, balancing task-specific improvements (TI) and the retention of generic knowledge (CC).

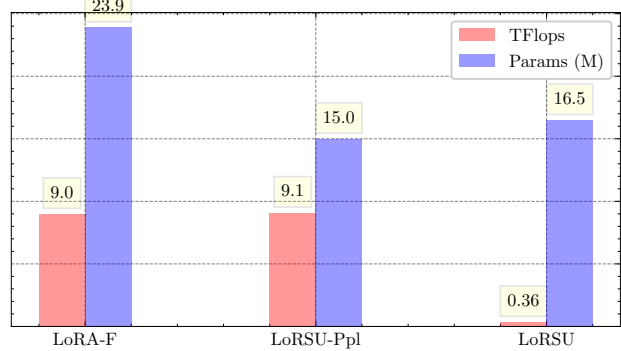


Figure 3. TFlops and trainable parameters comparison between LoRSU with CLIP loss (LoRSU), perplexity loss (LoRSU-Ppl), and LoRA-F.

Random selection (LoRSU-Rand) fails to generalize well, while fine-tuning all attention heads (LoRSU-AAH) adds unnecessary computational overhead with less effective generalization. LoRSU outperforms both of the variants in TI while LoRSU-AAH is marginally better in CC. Additional experiments that investigate the robustness of LoRSU in terms of the number of training epochs can be found in appendix E.3; ablation studies of other hyperparameters of LoRSU are given in appendix E.

4.6. Computational Efficiency

In Figure 3, we assess the computational benefits of LoRSU using the CLIP loss comparing to baseline methods. We focus on two key metrics: trainable parameters and floating-point operations per second (TFLOPs).

LoRSU requires $25\times$ fewer computation resources than LoRA-F and LoRSU-Ppl, demonstrating the suitability of using CLIP loss when computational resources are limited. Unlike the perplexity loss, which necessitates forward and backward passes through both the vision encoder and LLM, the CLIP loss operates solely on the vision encoder, significantly reducing computational overhead. This makes LoRSU more scalable, enabling efficient continual learning even in resource-constrained environments.

5. Discussion

In this work, we introduced LoRSU, a novel parameter-efficient fine-tuning method, specifically designed for few-shot continual learning scenarios with VLMs. Unlike existing approaches, LoRSU operates without relying on a replay buffer, making it uniquely suited for resource-constrained settings. Through extensive experiments, we demonstrate that LoRSU achieves both computational efficiency and the preservation of the model’s generic knowledge by using

localized and structured updates. LoRSU outperforms 12 baselines in over 80% of evaluations across 10 datasets and 3 settings, achieving the highest TI accuracies in most cases while maintaining stable or even positive CC accuracies. To the best of our knowledge, we are the first to explore few-shot continual learning of VLMs.

Whilst we focus on CLIP and LLaVA due to computational constraints, our method is generic to any transformer model, and we plan to extend it to other VLMs and image encoders. Another promising direction is using a smaller LLM proxy model in perplexity-based methods like LoRSU-Ppl, which has shown strong VQA performance. This could improve scalability and LoRSU’s use in resource-limited settings. Finally, LoRSU’s binary mask-based structured updates ensure efficient, precise parameter updates, but scaling to larger architectures like LLMs poses challenges. Replacing binary masks with more scalable solutions for vast parameter spaces will be crucial to manage memory and processing demands, offering opportunities for further refinement.

Impact Statement

Authors are **required** to include a statement of the potential broader impact of their work, including its ethical aspects and future societal consequences. This statement should be in an unnumbered section at the end of the paper (co-located with Acknowledgements – the two may appear in either order, but both must be before References), and does not count toward the paper page limit. In many cases, where the ethical impacts and expected societal implications are those that are well established when advancing the field of Machine Learning, substantial discussion is not required, and a simple statement such as the following will suffice:

“This paper presents work whose goal is to advance the field of Machine Learning. There are many potential societal consequences of our work, none which we feel must be specifically highlighted here.”

The above statement can be used verbatim in such cases, but we encourage authors to think about whether there is content which does warrant further discussion, as this statement will be apparent if the paper is later flagged for ethics review.

References

- Chaudhry, A., Dokania, P. K., Ajanthan, T., and Torr, P. H. Riemannian walk for incremental learning: Understanding forgetting and intransigence. In *Proceedings of the European conference on computer vision (ECCV)*, pp. 532–547, 2018.
- Chen, J., Zhu, D., Shen, X., Li, X., Liu, Z., Zhang, P., Krishnamoorthi, R., Chandra, V., Xiong, Y., and Elhoseiny, M. Minigpt-v2: large language model as a unified interface for vision-language multi-task learning. *arXiv preprint arXiv:2310.09478*, 2023.
- Chen, Z., Wu, J., Wang, W., Su, W., Chen, G., Xing, S., Zhong, M., Zhang, Q., Zhu, X., Lu, L., et al. Internvl: Scaling up vision foundation models and aligning for generic visual-linguistic tasks. In *Proceedings of the IEEE/CVF Conference on Computer Vision and Pattern Recognition*, pp. 24185–24198, 2024.
- Cheng, S., Tian, B., Liu, Q., Chen, X., Wang, Y., Chen, H., and Zhang, N. Can we edit multimodal large language models? In Bouamor, H., Pino, J., and Bali, K. (eds.), *Proceedings of the 2023 Conference on Empirical Methods in Natural Language Processing*, pp. 13877–13888, Singapore, December 2023. Association for Computational Linguistics. doi: 10.18653/v1/2023.emnlp-main.856. URL <https://aclanthology.org/2023.emnlp-main.856/>.
- Chiang, W.-L., Li, Z., Lin, Z., Sheng, Y., Wu, Z., Zhang, H., Zheng, L., Zhuang, S., Zhuang, Y., Gonzalez, J. E., et al. Vicuna: An open-source chatbot impressing gpt-4 with 90%* chatgpt quality. See <https://vicuna.lmsys.org> (accessed 14 April 2023), 2(3):6, 2023.
- Dai, D., Dong, L., Hao, Y., Sui, Z., Chang, B., and Wei, F. Knowledge neurons in pretrained transformers. *arXiv preprint arXiv:2104.08696*, 2021.
- Das, D., Talon, D., Mancini, M., Wang, Y., and Ricci, E. One vlm to keep it learning: Generation and balancing for data-free continual visual question answering. *arXiv preprint arXiv:2411.02210*, 2024.
- Das, S., Dai, R., Koperski, M., Minciullo, L., Garattoni, L., Bremond, F., and Francesca, G. Toyota smarthome: Real-world activities of daily living. In *Proceedings of the IEEE/CVF international conference on computer vision*, pp. 833–842, 2019.
- De Lange, M., Aljundi, R., Masana, M., Parisot, S., Jia, X., Leonardis, A., Slabaugh, G., and Tuytelaars, T. A continual learning survey: Defying forgetting in classification tasks. *IEEE transactions on pattern analysis and machine intelligence*, 44(7):3366–3385, 2021.
- Deng, J., Dong, W., Socher, R., Li, L.-J., Li, K., and Fei-Fei, L. ImageNet: A large-scale hierarchical image database. In *2009 IEEE Conference on Computer Vision and Pattern Recognition*, pp. 248–255, 2009. doi: 10.1109/CVPR.2009.5206848.
- Duan, H., Yang, J., Qiao, Y., Fang, X., Chen, L., Liu, Y., Dong, X., Zang, Y., Zhang, P., Wang, J., et al. Vlmevalkit: An open-source toolkit for evaluating large multi-modality models. In *Proceedings of the 32nd*

- ACM International Conference on Multimedia, pp. 11198–11201, 2024.
- Goswami, D., Twardowski, B., and Van De Weijer, J. Calibrating higher-order statistics for few-shot class-incremental learning with pre-trained vision transformers. In *Proceedings of the IEEE/CVF Conference on Computer Vision and Pattern Recognition*, pp. 4075–4084, 2024.
- He, H., Cai, J., Zhang, J., Tao, D., and Zhuang, B. Sensitivity-aware visual parameter-efficient fine-tuning. In *Proceedings of the IEEE/CVF International Conference on Computer Vision*, pp. 11825–11835, 2023a.
- He, J., Guo, H., Tang, M., and Wang, J. Continual instruction tuning for large multimodal models. *arXiv preprint arXiv:2311.16206*, 2023b.
- Helber, P., Bischke, B., Dengel, A., and Borth, D. Eurosat: A novel dataset and deep learning benchmark for land use and land cover classification. *IEEE Journal of Selected Topics in Applied Earth Observations and Remote Sensing*, 2019.
- Hu, E. J., Shen, Y., Wallis, P., Allen-Zhu, Z., Li, Y., Wang, S., Wang, L., and Chen, W. Lora: Low-rank adaptation of large language models. *arXiv preprint arXiv:2106.09685*, 2021.
- Kamoi, R., Zhang, Y., Das, S. S. S., Zhang, R. H., and Zhang, R. Visonlyqa: Large vision language models still struggle with visual perception of geometric information. *arXiv preprint arXiv:2412.00947*, 2024.
- Kiela, D., Firooz, H., Mohan, A., Goswami, V., Singh, A., Ringshia, P., and Testuggine, D. The hateful memes challenge: Detecting hate speech in multimodal memes. *Advances in neural information processing systems*, 33: 2611–2624, 2020.
- Kingma, D. P. Adam: A method for stochastic optimization. *arXiv preprint arXiv:1412.6980*, 2014.
- Kirkpatrick, J., Pascanu, R., Rabinowitz, N., Veness, J., Desjardins, G., Rusu, A. A., Milan, K., Quan, J., Ramalho, T., Grabska-Barwinska, A., et al. Overcoming catastrophic forgetting in neural networks. *Proceedings of the National Academy of Sciences*, 114(13):3521–3526, 2017.
- Li, J., Li, D., Savarese, S., and Hoi, S. Blip-2: Bootstrapping language-image pre-training with frozen image encoders and large language models. In *International conference on machine learning*, pp. 19730–19742. PMLR, 2023.
- Liu, F., Emerson, G. E. T., and Collier, N. Visual spatial reasoning. *Transactions of the Association for Computational Linguistics*, 2023.
- Liu, H., Li, C., Li, Y., Li, B., Zhang, Y., Shen, S., and Lee, Y. J. Llava-next: Improved reasoning, ocr, and world knowledge, 2024a.
- Liu, H., Li, C., Wu, Q., and Lee, Y. J. Visual instruction tuning. *Advances in neural information processing systems*, 36, 2024b.
- Lopez-Paz, D. and Ranzato, M. Gradient episodic memory for continual learning. *Advances in neural information processing systems*, 30, 2017.
- Loshchilov, I. Decoupled weight decay regularization. *arXiv preprint arXiv:1711.05101*, 2017.
- Maji, S., Kannala, J., Rahtu, E., Blaschko, M., and Vedaldi, A. Fine-grained visual classification of aircraft. Technical report, University of Oxford, 2013.
- Meng, K., Bau, D., Andonian, A., and Belinkov, Y. Locating and editing factual associations in gpt. *Advances in Neural Information Processing Systems*, 35:17359–17372, 2022.
- Mitchell, E., Lin, C., Bosselut, A., Finn, C., and Manning, C. D. Fast model editing at scale. In *International Conference on Learning Representations*, 2022. URL <https://openreview.net/forum?id=0DcZxewfOOpt>.
- Panos, A., Kobe, Y., Reino, D. O., Aljundi, R., and Turner, R. E. First session adaptation: A strong replay-free baseline for class-incremental learning. In *Proceedings of the IEEE/CVF International Conference on Computer Vision*, pp. 18820–18830, 2023.
- Paszke, A., Gross, S., Massa, F., Lerer, A., Bradbury, J., Chanan, G., Killeen, T., Lin, Z., Gimelshein, N., Antiga, L., et al. Pytorch: An imperative style, high-performance deep learning library. *Advances in Neural Information Processing Systems*, 32, 2019.
- Perez, E., Strub, F., De Vries, H., Dumoulin, V., and Courville, A. FiLM: Visual reasoning with a general conditioning layer. In *Proceedings of the AAAI Conference on Artificial Intelligence*, volume 32, 2018.
- Radford, A., Kim, J. W., Hallacy, C., Ramesh, A., Goh, G., Agarwal, S., Sastry, G., Askell, A., Mishkin, P., Clark, J., et al. Learning transferable visual models from natural language supervision. In *International conference on machine learning*, pp. 8748–8763. PMLR, 2021.
- Sinitsin, A., Plokhotnyuk, V., Pyrkin, D., Popov, S., and Babenko, A. Editable neural networks. In *International Conference on Learning Representations*, 2020. URL <https://openreview.net/forum?id=HJedXaEtvS>.

- Srivastava, S., Harun, M. Y., Shrestha, R., and Kanan, C. Improving multimodal large language models using continual learning. *arXiv preprint arXiv:2410.19925*, 2024.
- Stallkamp, J., Schlipsing, M., Salmen, J., and Igel, C. Man vs. computer: Benchmarking machine learning algorithms for traffic sign recognition. *Neural networks*, 32: 323–332, 2012.
- Tong, S., Liu, Z., Zhai, Y., Ma, Y., LeCun, Y., and Xie, S. Eyes wide shut? exploring the visual shortcomings of multimodal llms. In *Proceedings of the IEEE/CVF Conference on Computer Vision and Pattern Recognition*, pp. 9568–9578, 2024.
- Touvron, H., Martin, L., Stone, K., Albert, P., Almahairi, A., Babaei, Y., Bashlykov, N., Batra, S., Bhargava, P., Bhosale, S., et al. Llama 2: Open foundation and fine-tuned chat models. *arXiv preprint arXiv:2307.09288*, 2023.
- Vaswani, A., Shazeer, N., Parmar, N., Uszkoreit, J., Jones, L., Gomez, A. N., Kaiser, Ł., and Polosukhin, I. Attention is all you need. *Advances in neural information processing systems*, 30, 2017.
- Verwimp, E., Aljundi, R., Ben-David, S., Bethge, M., Cossu, A., Gepperth, A., Hayes, T. L., Hüllermeier, E., Kanan, C., Kudithipudi, D., et al. Continual learning: Applications and the road forward. *arXiv preprint arXiv:2311.11908*, 2023.
- Wang, P., Bai, S., Tan, S., Wang, S., Fan, Z., Bai, J., Chen, K., Liu, X., Wang, J., Ge, W., Fan, Y., Dang, K., Du, M., Ren, X., Men, R., Liu, D., Zhou, C., Zhou, J., and Lin, J. Qwen2-vl: Enhancing vision-language model’s perception of the world at any resolution. *arXiv preprint arXiv:2409.12191*, 2024a.
- Wang, Q., Lin, Y., Chen, Y., Schmidt, L., Han, B., and Zhang, T. Do clips always generalize better than imagenet models? *arXiv preprint arXiv:2403.11497*, 2024b.
- Wu, T., Luo, L., Li, Y.-F., Pan, S., Vu, T.-T., and Haffari, G. Continual learning for large language models: A survey. *arXiv preprint arXiv:2402.01364*, 2024.
- Zhang, Q., Chen, M., Bukharin, A., Karampatziakis, N., He, P., Cheng, Y., Chen, W., and Zhao, T. Adalora: Adaptive budget allocation for parameter-efficient fine-tuning. *arXiv preprint arXiv:2303.10512*, 2023.
- Zhang, W., Janson, P., Aljundi, R., and Elhoseiny, M. Overcoming generic knowledge loss with selective parameter update. In *Proceedings of the IEEE/CVF Conference on Computer Vision and Pattern Recognition*, pp. 24046–24056, 2024.
- Zhao, L., Zhang, X., Yan, K., Ding, S., and Huang, W. Safe: Slow and fast parameter-efficient tuning for continual learning with pre-trained models. *arXiv preprint arXiv:2411.02175*, 2024.
- Zhu, D., Chen, J., Shen, X., Li, X., and Elhoseiny, M. Minigpt-4: Enhancing vision-language understanding with advanced large language models. *arXiv preprint arXiv:2304.10592*, 2023.

A. Proof of the optimal mask \mathbf{p}^*

Definition A.1. The operator $\text{TOP-}C : \mathbb{R}^d \rightarrow \mathbb{R}^d$, for $1 \leq C \leq d$ is defined as

$$(\text{TOP-}C(\mathbf{x}))_{\pi(i)} := \begin{cases} x_{\pi(i)}, & i \leq C \\ 0, & \text{otherwise,} \end{cases}$$

where $\mathbf{x} = (x_1, \dots, x_d)^\top \in \mathbb{R}^d$ and π is a permutation of $\{1, 2, \dots, d\}$ such that $|x_{\pi(i)}| \geq |x_{\pi(i+1)}|$, for $i = 1, \dots, d-1$, i.e. the $\text{TOP-}S$ operator keeps only the S largest elements of \mathbf{x} in magnitude and truncates the rest to zero.

Lemma A.2. For any $\mathbf{x} \in \mathbb{R}^d - \{\mathbf{0}\}$, $1 \leq C \leq d$, the optimal mask

$$\mathbf{p}^* = \arg \max_{\mathbf{p} \in \{0,1\}^d} \frac{\|\mathbf{p} \odot \mathbf{x}\|^2}{\|\mathbf{x}\|^2}, \quad \text{s.t. } \|\mathbf{p}\|_0 \leq C,$$

has zeros everywhere except the C largest elements of \mathbf{x} in magnitude.

Proof. Rewriting the optimization problem as

$$\max_{\mathbf{p} \in \{0,1\}^d} \sum_{i=1}^d p_i x_i^2, \quad \text{s.t. } \sum_{i=1}^d p_i \leq C,$$

Notice that this is a trivial binary knapsack problem with maximum weight capacity C and weights equal to one. Hence, the maximum is attained when we pick the top C maximal x_i^2 elements. \square

Remark A.3.

It holds that $\text{TOP-}S(\mathbf{x}) = \mathbf{p}^* \odot \mathbf{x}$.

Corollary A.4. The optimal mask \mathbf{p}^* in (6) has zeros everywhere except for the indices $i \in \{j : \exists \ell \in \{1, \dots, G\}, \text{ such that } j \in \{\pi_\ell(1), \dots, \pi_\ell(c_\ell)\}\}$, where π_ℓ is the same permutation as in Definition A.1 for the set of indices I_ℓ .

Proof. The result follows from the mutual exclusiveness of I_ℓ in the constraints of (6) and Lemma A.2. \square

B. Implementation Details

We describe below the implementation details of section 4.

- All the experiments are conducted on a single NVIDIA A100 GPU.
- We have included error bars over three runs for all experiments.
- We use PyTorch (Paszke et al., 2019) to implement all the algorithms.
- We use Adam (Kingma, 2014) as an optimizer for the methods that utilize the CLIP loss for fine tuning and AdamW (Loshchilov, 2017) for those ones that use the perplexity loss.
- A learning rate scheduler of Cosine Annealing with Warmup is employed for all methods.
- For all experiments, we set the learning rate 1×10^{-5} and 2×10^{-5} , for LoRSU and LoRSU-Ppl, respectively.
- We set batch size to 16 for all methods that fine-tune the vision encoder through CLIP loss. We reduce the batch size to 8 for those methods that fine-tune the vision encoder through perplexity loss or those that fine-tune the LLM. This was due to GPU memory limitations.
- All methods run for 20, 15, and 10 epochs for the CL-5, CL-10, and CL-50 settings, respectively.
- For LoRA (-Ppl), we set rank $r = 64$ while LoRA-L and LoRA-F use $r = 8$, for all experiments.

- For AdaLoRA, we set the initial rank to 70 and the final average rank to 64.
- The adapters of LoRA and AdaLoRA are applied to all weight matrices of each of the transformer blocks.
- For SPU, we use sparsity=15% for all experiments.
- For LoRSU (-Ppl) we use sparsity=10%, rank=64, and we pick the top-2 attention heads for all experiments.

The choice of the above hyperparameters ensures that LoRA (-Ppl), LoRA-L, LoRA-F, AdaLoRA, SPU, and LoRSU (-Ppl) have similar number of trainable parameters.

C. Datasets

Details on all datasets used in section 4 are presented here.

C.1. TSI & DALLE

We start with the description of how we constructed our newly introduced VQA datasets *TSI* and *DALLE*.

TSI. To extract images from the videos of the Toyota Smart Home dataset (TSI), we discretized each video clip into 2 frames per second and then selected the frame in the middle of the total time duration of the video clip. In Table 5 we describe the actions that were selected and the corresponding prompt used for CLIP classification. We also note dropping few actions to avoid ambiguous classes.

DALLE. We generated images from DALL-E 2 using OpenAI python package and we used the prompt “A person {*a*}” where *a* ∈ { *using a white coffee machine, eating, cutting bread, stirring the pot, holding a glass, watching TV, holding a bottle, walking, making tea, cutting food, holding a cup, using a laptop, lying down, holding a can, person holding a black kettle, reading a book, cleaning up, sitting down, using a tablet, boiling water in a black kettle, using a cordless phone, washing dishes*}.

In Table 6, we present the average number of images per session used to update the model for each CL setting. Finally, Table 7 provides characteristics of the datasets used for evaluating performance.

C.2. Continual Learning Splits

For the continual learning settings of section 4, we split all datasets into five non-overlapping continual learning (CL) splits based on the classes/categories of each dataset. Unless stated otherwise, we use the training split of each dataset to construct these CL splits.

GTS (Stallkamp et al., 2012). We split the 43 classes of GTS as follows:

- *Session 1:* [25, 2, 11, 1, 40, 27, 5, 9, 17].
- *Session 2:* [32, 29, 20, 39, 21, 15, 23, 10, 3].
- *Session 3:* [18, 38, 42, 14, 22, 35, 34, 19, 33].
- *Session 4:* [12, 26, 41, 0, 37, 6, 13, 24].
- *Session 5:* [30, 28, 31, 7, 16, 4, 36, 8].

TSI (Das et al., 2019). We split the 27 action categories of TSI as follows:

- *Session 1:* [WatchTV, Laydown, Sitdown, PourFromkettle, Enter, DrinkFrombottle].
- *Session 2:* [EatAttalbe, PourFrombottle, CookCleandishes, MaketeaBoilwater, Leave, CookCleanup].
- *Session 3:* [MaketeaInsertteabag, MakecoffeePourwater, DrinkFromcan, Readbook, Cutbread].

Table 5. The original action names of the Toyota Smarthome dataset and their corresponding captions used to create the Toyota Smarthome Images (TSI) dataset. We use \times to denote the actions that are ambiguous and were not used to build the TSI dataset. The final prompt is created as “*The person in this image is {caption}*”.

Original Class name/Action	Generated Caption
Cook.Cleandishes	washing dishes
Cook.Cleanup	cleaning up
Cook.Cut	cutting food
Cook.Stir	stirring the pot
Cook.Usestove	\times
Cook.Cutbread	cutting bread
Drink.Frombottle	holding a bottle
Drink.Fromcan	holding a can
Drink.Fromcup	holding a cup
Drink.Fromglass	holding a glass
Eat.Attable	eating
Eat.Snack	\times
Enter	walking
Getup	\times
Laydown	lying down
Leave	walking
Makecoffee.Pourgrains	using a white coffee machine
Makecoffee.Pourwater	using a white coffee machine
Maketea.Boilwater	boiling water in a black kettle
Maketea.Insertteabag	making tea
Pour.Frombottle	holding a bottle
Pour.Fromcan	holding a can
Pour.Fromkettle	holding a black kettle
Readbook	reading a book
Sitdown	sitting down
Takepills	\times
Uselaptop	using a laptop
Usetablet	using a tablet
Usetelephone	using a cordless phone
Walk	walking
WatchTV	watching TV

- *Session 4:* [*Drink.Fromcup*, *Drink.Fromglass*, *Usetablet*, *Pour.Fromcan*, *Usetelephone*].
- *Session 5:* [*Walk*, *Cook.Stir*, *Makcoffe.Pourgrains*, *Cook.Cut*, *Uselaptop*].

CAn (Wang et al., 2024b). The 45 classes of CAn are split as follows:

- *Session 1:* [102, 9, 20, 56, 23, 30, 357, 291, 144].
- *Session 2:* [41, 293, 42, 49, 54, 57, 70, 279, 305].
- *Session 3:* [71, 10, 76, 79, 349, 16, 81, 83, 100].
- *Session 4:* [130, 30, 133, 150, 275, 276, 58, 277, 80].
- *Session 5:* [39, 290, 37, 296, 316, 337, 89, 360, 128].

The indices of CAn correspond to those of ImageNet (Deng et al., 2009) since the dataset was built based on these 45 animal classes of ImageNet.

AIR (Maji et al., 2013). We split the 100 aircraft types of AIR as follows:

- *Session 1:* [23, 8, 11, 7, 48, 13, 1, 91, 94, 54, 16, 63, 52, 41, 80, 2, 47, 87, 78, 66].
- *Session 2:* [19, 6, 24, 10, 59, 30, 22, 29, 83, 37, 93, 81, 43, 99, 86, 28, 34, 88, 44, 14].
- *Session 3:* [84, 70, 4, 20, 15, 21, 31, 76, 57, 67, 73, 50, 69, 25, 98, 46, 96, 0, 72, 35].
- *Session 4:* [58, 92, 3, 95, 56, 90, 26, 40, 55, 89, 75, 71, 60, 42, 9, 82, 39, 18, 77, 68].
- *Session 5:* [32, 79, 12, 85, 36, 17, 64, 27, 74, 45, 61, 38, 51, 62, 65, 33, 5, 53, 97, 49].

ESAT (Helber et al., 2019). We split the 10 different land terrain classes of ESAT as follows:

- *Session 1:* [0, 1].
- *Session 2:* [2, 3].
- *Session 3:* [4, 5].
- *Session 4:* [6, 7].
- *Session 5:* [8, 9].

DALLE. This dataset was only used for performance evaluation (control dataset), and not fine-tuning.

VSR (Liu et al., 2023). The images of this VQA dataset are labeled according to 36 different categories that describe the dominant object of the image. We create the CL splits as follows:

- *Session 1:* [*oven*, *dining table*, *spoon*, *boat*, *cake*, *donut*, *sandwich*].
- *Session 2:* [*fire hydrant*, *elephant*, *airplane*, *truck*, *apple*, *hot dog*, *sheep*].
- *Session 3:* [*kite*, *baseball glove*, *cow*, *tie*, *scissors*, *toaster*, *tv*].
- *Session 4:* [*bicycle*, *banana*, *couch*, *teddy bear*, *bus*, *umbrella*, *bird*].
- *Session 5:* [*potted plant*, *bowl*, *broccoli*, *bottle*, *knife*, *orange*, *person*, *pizza*].

Table 6. Average number of images per session (5 sessions in total) for each dataset used for fine-tuning.

Setting	FT Dataset							
	GTS	TSI	CAn	AIR	ESAT	VSR	HM	VisOnly
CL-5	43.0	27.0	45.0	100.0	10.0	100.0	100.0	7.0
CL-20	170.0	84.0	180.0	400.0	40.0	274.6	300.0	28.0
CL-50	430.0	253.8	450.0	1000.0	100.0	485.2	600.0	70.0

Table 7. Characteristics of the datasets used for performance evaluation in section 4.

Eval Datasets	GTS	TSI	CAn	AIR	ESAT	DALLE	VSR	HM	MMVP	VisOnly
# Samples	3,990	4,908	1,796	3,333	17,000	660	1,222	2,000	150	1,150
# Classes	43	27	45	100	10	27	36	NaN	NaN	7

HM (Kiela et al., 2020). For the hateful memes dataset, since there was not any labeling information of the images so we can split the images in a meaningful way, we randomly split the training images into five disjoint sets to create our final CL splits.

MMVP (Tong et al., 2024). This is the only dataset where no training split is available and it is comprised of just 300 images. For this reason, we only used it for evaluation in our experiments in the main paper. However, for completeness, we included results in Table 21 where we fine-tune on it. We use 150 images for training which are equally split into five sessions and the rest of the 150 images are used for evaluation. Thus, the setting can be considered as a 30-shot CL setting.

VisOnly (Kamoi et al., 2024). This dataset categorizes its samples into seven categories describing the nature of the geometric and numerical information in scientific figures. We created the splits as follows:

- Session 1: *Geometry-Triangle*.
- Session 2: *Geometry-Quadrilateral*.
- Session 3: *Geometry-Length*
- Session 4: *Geometry-Angle*.
- Session 5: [*Geometry-Area*, *3D-Size*, *3D-Angle*].

D. Detailed Results

D.1. CLIP-based Updates+

The detailed accuracies for all baselines and datasets used to create Table 1 of the main paper can be found in Tables 8 through 12.

D.2. Extra ACC and BWT results

In Table 13 we present results of the ACC and BWT on extra datasets plus the ones in the main paper. The results follow the same patterns as in section 4 with LoRSU demonstrating the most consistent performance in both ACC and BWT compared to the other two baselines. SPU is close to LoRSU in terms of BWT but it significantly lags behind in ACC.

Table 8. Accuracy scores (%) for LLaVA with the pretrained (*Zr-Shot*) or fine-tuned image encoder. All baselines use *GTS* dataset for fine-tuning the image encoder (the LLM remains frozen) via CLIP loss. We include error bars over 3 runs.

		VQA Datasets (Acc %)									
Setting	FT Method	GTS	TSI	CAn	AIR	ESAT	DALLE	VSR	HM	MMVP	VisOnly
CL-5	Zr-Shot	75.6	53.1	82.7	60.4	76.1	91.1	51.5	61.2	58.0	31.3
	LN	79.1±1.2	53.6±0.5	81.2±0.6	61.0±1.2	58.9±0.9	91.1±1.3	51.9±1.5	62.7±1.1	59.6±0.2	31.8±0.4
	F-FT	79.3±0.6	55.1±0.8	76.8±1.3	58.8±1.0	25.6±0.9	89.2±1.2	51.7±0.9	62.1±0.8	56.4±0.4	30.9±0.2
	F-EWC	80.6±0.6	37.4±1.3	63.2±0.7	55.8±1.4	26.1±1.4	81.5±1.1	51.8±1.4	61.2±0.6	53.8±0.4	31.2±0.4
	LoRA	76.3±0.8	52.6±1.4	73.3±0.6	56.7±1.2	49.3±0.8	87.1±1.3	51.8±1.2	61.3±1.2	58.1±0.3	31.6±0.4
	AdaLoRA	74.7±0.9	49.7±0.7	79.6±0.9	56.3±0.8	42.5±0.8	91.6±1.1	52.0±0.8	60.9±1.2	57.1±0.3	31.7±0.2
	SPU	81.0±1.4	53.7±1.5	82.5±0.7	61.0±1.0	67.8±0.6	91.6±1.3	52.0±0.6	62.0±1.3	58.2±0.2	31.6±0.2
	LoRSU	82.0±1.3	53.5±1.3	82.4±0.8	60.8±1.4	66.6±0.9	91.5±1.4	51.6±0.7	61.7±1.4	59.8±0.2	31.6±0.2
CL-20	LN	80.8±0.6	49.5±0.7	77.7±1.0	59.7±0.5	32.7±0.6	89.8±0.9	51.8±0.7	62.3±0.3	57.5±0.1	31.2±0.2
	F-FT	80.2±0.8	54.5±0.7	74.9±0.8	57.2±1.0	23.2±0.7	86.7±0.4	51.9±0.9	61.6±1.0	58.3±0.2	31.7±0.3
	F-EWC	82.3±0.9	35.5±0.9	55.7±0.4	35.4±0.3	28.7±0.9	72.4±0.8	51.6±0.7	60.9±0.8	53.5±0.2	31.0±0.3
	LoRA	78.1±0.8	55.6±0.3	59.0±0.9	47.6±0.4	26.0±0.6	83.6±0.8	52.1±0.5	62.1±1.0	53.7±0.3	30.8±0.2
	AdaLoRA	75.8±0.8	51.9±0.5	79.3±0.9	59.3±0.4	62.1±0.4	90.7±1.0	51.6±0.5	61.1±0.6	57.7±0.2	31.7±0.2
	SPU	83.5±0.6	53.1±0.6	82.2±0.7	60.7±0.8	62.0±0.4	91.5±0.4	51.9±0.5	61.8±0.7	58.8±0.2	31.5±0.2
	LoRSU	84.2±0.9	52.9±0.6	82.2±0.5	60.7±0.6	64.7±0.6	90.8±0.5	51.9±0.4	61.7±0.5	59.5±0.1	31.6±0.2
	LN	80.4±0.2	50.4±0.1	74.9±0.1	58.3±0.0	30.4±0.3	89.0±0.1	51.8±0.0	62.0±0.3	58.7±0.1	31.4±0.1
CL-50	F-FT	79.0±0.1	48.9±0.2	65.0±0.2	55.0±0.3	23.5±0.0	86.8±0.2	52.0±0.1	60.8±0.1	54.9±0.1	30.7±0.1
	F-EWC	80.9±0.2	45.2±0.4	60.5±0.4	43.2±0.0	26.9±0.3	78.5±0.1	52.0±0.0	58.7±0.1	52.9±0.0	31.7±0.1
	LoRA	78.7±0.0	50.7±0.0	62.1±0.2	47.4±0.1	24.2±0.2	82.9±0.3	51.7±0.3	61.0±0.2	54.3±0.1	30.8±0.0
	AdaLoRA	76.6±0.4	50.4±0.0	79.0±0.2	57.4±0.1	58.3±0.1	90.4±0.2	51.6±0.2	61.8±0.3	55.4±0.1	31.8±0.1
	SPU	83.3±0.3	53.8±0.2	81.8±0.2	61.1±0.4	58.8±0.0	91.0±0.2	51.8±0.4	62.1±0.1	59.5±0.1	32.2±0.1
	LoRSU	85.3±0.1	54.2±0.1	81.9±0.2	60.5±0.2	61.4±0.3	91.0±0.1	51.7±0.2	62.2±0.4	58.9±0.1	31.8±0.1

Table 9. Accuracy scores (%) for LLaVA with the pretrained (*Zr-Shot*) or fine-tuned image encoder. All baselines use *TSI* dataset for fine-tuning the image encoder (the LLM remains frozen) via CLIP loss. We include error bars over 3 runs.

		VQA Datasets (Acc %)									
Setting	FT Method	GTS	TSI	CAn	AIR	ESAT	DALLE	VSR	HM	MMVP	VisOnly
CL-5	Zr-Shot	75.6	53.1	82.7	60.4	76.1	91.1	51.5	61.2	58.0	31.3
	LN	75.4±1.0	53.9±0.6	82.6±1.3	60.0±1.0	75.9±0.8	91.1±1.3	51.7±1.4	61.9±1.0	58.4±0.3	30.9±0.3
	F-FT	73.8±0.5	60.5±1.1	81.6±0.9	59.5±1.5	70.4±1.0	91.1±1.2	51.8±0.9	61.5±1.3	56.9±0.2	31.3±0.3
	F-EWC	74.9±1.1	61.6±1.0	82.1±1.1	58.8±0.9	72.3±1.2	89.9±1.4	51.9±0.9	62.4±1.4	55.5±0.4	31.5±0.3
	LoRA	73.4±1.0	53.0±0.9	80.2±0.6	58.8±0.7	59.1±1.4	90.2±1.1	51.6±1.3	61.2±1.4	56.7±0.4	31.7±0.4
	AdaLoRA	75.6±0.8	54.2±0.6	82.6±1.1	60.0±1.3	75.7±1.3	91.1±1.2	51.6±0.9	62.1±1.0	59.5±0.3	31.7±0.2
	SPU	75.4±0.7	54.0±1.1	83.0±1.3	60.1±0.6	75.7±1.5	91.3±1.3	51.9±1.4	61.7±0.9	58.5±0.4	31.6±0.4
	LoRSU	75.9±0.9	56.3±0.7	82.7±0.9	60.8±1.0	76.2±1.4	91.3±1.2	51.6±0.9	61.7±0.8	57.7±0.3	31.2±0.3
CL-20	LN	72.9±0.5	58.2±0.5	78.9±0.9	56.8±0.4	69.3±0.9	91.4±0.8	51.6±0.8	62.6±0.5	56.3±0.3	31.3±0.2
	F-FT	72.1±0.7	68.4±0.4	80.0±0.7	55.4±0.4	58.8±0.8	88.4±0.3	51.8±0.6	62.3±0.5	56.9±0.2	31.2±0.3
	F-EWC	23.3±0.6	69.1±0.6	20.4±0.7	20.1±0.6	24.2±0.6	17.7±0.7	51.7±0.7	56.9±0.8	49.6±0.3	31.1±0.1
	LoRA	68.5±0.7	61.6±0.3	76.7±0.9	55.3±0.7	55.6±0.6	88.8±0.8	51.9±0.3	61.4±0.6	59.1±0.3	31.1±0.3
	AdaLoRA	70.3±0.5	54.4±0.4	72.4±0.5	43.6±0.8	34.6±0.7	77.0±0.3	52.2±0.9	62.6±0.4	57.0±0.1	31.9±0.3
	SPU	75.5±0.7	60.9±0.8	82.3±0.4	59.2±0.5	73.7±1.0	91.2±0.7	51.7±0.8	61.8±0.9	58.2±0.3	32.0±0.2
	LoRSU	75.9±0.6	63.7±0.4	82.8±0.8	60.4±0.3	73.4±0.6	90.9±0.6	51.7±0.4	61.5±0.7	58.8±0.2	31.9±0.2
	LN	73.0±0.2	60.1±0.2	79.6±0.3	57.7±0.4	61.3±0.4	89.6±0.4	51.9±0.0	61.3±0.0	55.5±0.1	31.3±0.1
CL-50	F-FT	72.5±0.4	70.3±0.1	78.3±0.4	53.4±0.0	50.6±0.2	89.1±0.3	52.3±0.3	61.1±0.2	57.1±0.1	31.7±0.0
	F-EWC	48.0±0.3	75.5±0.2	59.5±0.4	38.8±0.1	42.6±0.3	82.5±0.0	52.5±0.1	56.4±0.3	55.4±0.1	31.3±0.1
	LoRA	66.1±0.2	71.3±0.3	76.0±0.1	56.0±0.1	44.5±0.2	88.9±0.3	51.8±0.1	60.4±0.2	56.3±0.1	31.6±0.1
	AdaLoRA	73.1±0.2	61.0±0.0	80.6±0.0	52.0±0.4	72.2±0.3	88.9±0.3	51.7±0.2	62.0±0.4	59.1±0.0	31.2±0.1
	SPU	75.4±0.0	65.3±0.1	81.8±0.1	59.7±0.2	72.3±0.1	90.8±0.2	51.9±0.1	61.9±0.4	58.0±0.1	31.8±0.0
	LoRSU	75.3±0.2	72.2±0.4	82.4±0.3	59.7±0.3	72.5±0.3	90.8±0.3	51.7±0.2	61.7±0.4	58.5±0.1	31.7±0.0

Table 10. Accuracy scores (%) for LLaVA with the pretrained (*Zr-Shot*) or fine-tuned image encoder. All baselines use *CAn* dataset for fine-tuning the image encoder (the LLM remains frozen) via CLIP loss. We include error bars over 3 runs.

		VQA Datasets (Acc %)									
Setting	FT Method	GTS	TSI	CAn	AIR	ESAT	DALLE	VSR	HM	MMVP	VisOnly
CL-5	Zr-Shot	75.6	53.1	82.7	60.4	76.1	91.1	51.5	61.2	58.0	31.3
	LN	74.3±1.5	52.9±1.4	80.3±1.4	58.9±0.7	72.4±1.2	91.1±0.8	52.0±0.9	61.5±1.2	61.7±0.3	32.1±0.4
	F-FT	73.5±1.1	50.6±0.9	80.3±0.8	56.5±0.6	63.1±0.6	91.3±1.5	51.7±1.4	61.8±0.8	58.4±0.2	31.3±0.4
	F-EWC	65.9±1.5	39.1±0.7	66.0±1.3	40.0±0.9	41.7±0.7	86.2±0.8	51.8±1.3	59.9±1.0	57.6±0.4	31.3±0.2
	LoRA	69.7±1.4	44.8±1.1	81.4±0.7	56.9±1.0	50.7±1.3	92.9±1.3	52.0±1.0	61.8±1.5	56.5±0.4	31.3±0.4
	AdaLoRA	75.5±1.4	53.2±0.7	81.7±0.6	60.1±0.7	72.0±1.2	92.1±0.9	51.9±1.4	61.8±1.5	59.0±0.3	31.9±0.3
	SPU	76.0±0.9	53.2±0.6	82.3±1.1	60.3±1.3	75.7±0.9	91.3±1.3	51.7±0.8	61.5±1.2	58.4±0.3	31.4±0.4
CL-20	LoRSU	75.2±0.8	52.7±0.9	83.0±1.0	60.1±0.7	76.8±1.0	91.8±1.4	51.6±1.1	62.3±1.2	58.7±0.3	31.4±0.4
	LN	72.9±0.5	54.0±0.9	80.3±0.6	57.3±0.4	73.3±0.4	90.7±0.4	51.8±0.8	61.9±0.9	61.0±0.1	31.4±0.1
	F-FT	72.9±0.5	47.9±0.6	83.0±0.7	56.9±0.9	62.7±0.9	90.6±0.9	51.9±0.4	61.3±0.4	56.5±0.2	31.5±0.3
	F-EWC	70.1±1.0	48.7±0.4	82.8±0.5	51.1±0.8	54.8±0.9	88.3±0.7	51.8±1.0	57.0±0.8	59.6±0.3	31.2±0.3
	LoRA	67.5±0.6	48.9±0.6	80.4±0.4	57.3±0.9	39.7±0.4	91.1±0.6	51.8±0.9	61.7±0.3	60.1±0.2	31.9±0.3
	AdaLoRA	72.5±1.0	51.5±1.0	79.2±0.4	54.1±1.0	65.5±0.7	90.6±0.8	51.7±0.9	61.9±0.9	56.5±0.3	31.7±0.3
	SPU	75.0±0.5	53.5±0.3	82.8±0.8	59.9±0.6	76.1±0.9	91.6±0.9	51.6±0.6	61.9±0.4	61.8±0.2	31.6±0.3
CL-50	LoRSU	75.3±0.8	53.1±0.9	83.8±0.9	58.8±1.0	75.5±0.7	92.0±0.3	51.9±0.4	62.3±0.6	60.4±0.2	31.6±0.2
	LN	71.1±0.1	50.4±0.3	77.0±0.3	57.5±0.3	57.9±0.1	89.7±0.1	51.6±0.1	62.4±0.3	56.1±0.1	31.9±0.0
	F-FT	70.1±0.1	48.9±0.3	81.7±0.0	56.2±0.2	47.5±0.1	89.9±0.3	52.0±0.1	61.2±0.1	57.7±0.1	31.1±0.1
	F-EWC	61.7±0.0	43.9±0.3	83.3±0.4	46.2±0.3	38.9±0.2	87.5±0.1	51.8±0.3	55.8±0.3	54.7±0.1	30.7±0.1
	LoRA	66.8±0.2	47.8±0.3	82.3±0.2	55.7±0.0	52.0±0.3	91.0±0.3	51.7±0.3	61.6±0.2	60.2±0.0	31.6±0.1
	AdaLoRA	73.5±0.0	49.9±0.1	80.9±0.4	55.7±0.4	77.8±0.1	93.1±0.0	51.5±0.1	61.4±0.3	56.9±0.0	31.6±0.1
	SPU	75.2±0.2	53.2±0.0	83.3±0.3	59.3±0.2	73.1±0.3	91.4±0.4	51.7±0.3	61.7±0.1	58.5±0.1	31.6±0.1
	LoRSU	75.0±0.2	51.8±0.1	84.0±0.4	58.5±0.2	72.7±0.3	91.9±0.3	51.7±0.1	62.3±0.4	58.1±0.0	31.7±0.1

Table 11. Accuracy scores (%) for LLaVA with the pretrained (*Zr-Shot*) or fine-tuned image encoder. All baselines use *AIR* dataset for fine-tuning the image encoder (the LLM remains frozen) via CLIP loss. We include error bars over 3 runs.

		VQA Datasets (Acc %)									
Setting	FT Method	GTS	TSI	CAn	AIR	ESAT	DALLE	VSR	HM	MMVP	VisOnly
CL-5	Zr-Shot	75.6	53.1	82.7	60.4	76.1	91.1	51.5	61.2	58.0	31.3
	LN	73.4±0.8	51.3±1.2	80.2±0.6	60.7±1.5	66.9±0.7	91.3±0.6	51.9±0.9	62.4±1.2	58.5±0.2	30.6±0.2
	F-FT	72.5±1.2	50.5±0.5	79.9±0.9	62.4±0.9	60.7±1.4	90.6±0.5	51.7±0.9	60.9±1.1	58.3±0.4	31.4±0.3
	F-EWC	74.9±1.2	52.4±0.8	71.5±1.2	63.3±1.0	63.8±1.0	90.7±1.5	51.2±0.5	61.2±0.8	58.1±0.4	31.4±0.4
	LoRA	70.9±0.9	52.7±0.6	79.0±0.7	61.7±0.5	48.8±0.7	90.6±0.6	52.0±0.9	62.5±0.8	60.0±0.3	31.1±0.2
	AdaLoRA	75.0±1.0	53.3±0.8	83.7±0.9	60.8±0.8	75.2±1.5	91.7±1.0	51.6±0.8	61.6±0.8	56.9±0.3	31.9±0.4
	SPU	76.2±0.6	53.0±1.3	83.0±0.8	63.5±0.8	75.3±0.7	91.5±1.5	51.5±0.6	61.5±0.8	58.1±0.3	31.5±0.4
CL-20	LoRSU	76.2±0.8	53.4±1.4	82.5±1.0	65.2±1.3	76.0±0.9	91.8±0.8	51.6±0.8	62.1±1.1	59.0±0.4	31.2±0.3
	LN	70.3±0.9	53.7±0.6	77.9±1.0	60.2±0.4	56.3±0.7	90.6±0.3	51.7±1.0	62.8±0.7	58.1±0.1	31.8±0.3
	F-FT	73.0±0.6	54.1±0.6	80.3±0.9	69.7±0.5	62.7±0.5	90.0±0.4	51.9±0.3	61.8±0.4	58.9±0.1	31.4±0.1
	F-EWC	71.2±0.5	53.9±1.0	79.3±0.4	70.6±1.0	64.6±0.7	89.7±0.6	51.7±0.4	61.5±0.5	58.9±0.3	31.4±0.2
	LoRA	71.8±0.9	51.1±0.8	78.6±0.3	65.7±0.4	63.4±0.8	89.9±1.0	51.7±0.3	62.3±0.3	56.2±0.2	31.5±0.2
	AdaLoRA	73.4±0.8	51.6±0.6	81.2±0.9	63.1±0.6	73.8±0.8	90.8±0.5	52.1±0.4	62.7±0.8	57.7±0.2	31.2±0.1
	SPU	75.7±0.4	52.2±0.7	82.0±0.8	63.4±0.9	72.6±0.6	91.7±0.6	51.8±0.6	62.2±0.5	59.0±0.2	31.4±0.2
CL-50	LoRSU	75.7±0.9	52.6±0.9	81.4±0.7	66.3±0.7	73.0±0.8	90.9±0.8	51.9±0.8	61.8±0.8	56.9±0.1	31.6±0.3
	LN	69.6±0.4	54.0±0.1	76.9±0.3	62.2±0.2	50.9±0.2	90.2±0.0	52.0±0.3	62.8±0.4	57.7±0.1	31.5±0.1
	F-FT	71.2±0.3	50.3±0.3	78.3±0.2	70.4±0.4	59.9±0.0	90.1±0.1	51.9±0.1	61.8±0.3	57.5±0.1	31.3±0.1
	F-EWC	71.8±0.2	51.6±0.1	78.3±0.0	71.3±0.2	57.6±0.2	90.2±0.2	51.7±0.1	61.1±0.2	57.4±0.1	31.5±0.0
	LoRA	69.8±0.0	54.7±0.0	77.0±0.3	68.2±0.3	51.6±0.1	90.0±0.1	52.0±0.4	62.4±0.0	57.1±0.1	31.5±0.1
	AdaLoRA	74.2±0.3	52.0±0.2	82.4±0.1	65.0±0.2	72.6±0.0	91.9±0.1	51.7±0.2	60.7±0.1	55.6±0.0	31.3±0.0
	SPU	75.2±0.2	52.2±0.4	82.6±0.3	66.6±0.4	70.0±0.2	91.6±0.3	51.9±0.2	62.0±0.3	57.6±0.0	31.8±0.0
	LoRSU	75.4±0.4	52.7±0.3	81.6±0.2	68.6±0.3	69.7±0.3	91.5±0.2	51.7±0.4	62.2±0.1	58.7±0.1	31.1±0.1

Table 12. Accuracy scores (%) for LLaVA with the pretrained (*Zr-Shot*) or fine-tuned image encoder. All baselines use *ESAT* dataset for fine-tuning the image encoder (the LLM remains frozen) via CLIP loss. We include error bars over 3 runs.

		VQA Datasets (Acc %)									
Setting	FT Method	GTS	TSI	CAn	AIR	ESAT	DALLE	VSR	HM	MMVP	VisOnly
CL-5	Zr-Shot	75.6	53.1	82.7	60.4	76.1	91.1	51.5	61.2	58.0	31.3
	LN	75.8±0.9	53.2±0.6	82.6±1.1	60.0±1.3	80.3±1.0	92.7±1.0	51.9±0.7	61.7±0.5	60.4±0.4	31.8±0.3
	F-FT	69.1±0.8	50.5±0.6	80.8±1.1	57.7±1.5	65.8±0.6	91.3±1.5	51.8±0.7	62.0±0.7	58.8±0.3	30.4±0.2
	F-EWC	66.3±0.9	52.1±1.4	79.3±1.0	56.8±1.3	67.7±1.3	90.9±0.8	51.9±1.3	62.0±1.2	55.4±0.2	30.9±0.4
	LoRA	73.2±1.3	49.3±1.2	80.6±0.9	60.4±1.1	74.5±0.8	92.3±1.3	52.0±1.1	61.6±1.1	57.4±0.4	31.4±0.3
	AdaLoRA	75.9±0.5	52.4±1.4	82.4±0.5	60.5±0.8	78.0±1.3	91.5±0.9	51.6±0.8	61.5±1.3	59.0±0.4	30.9±0.2
	SPU	75.8±0.8	53.2±1.4	82.8±1.4	60.5±1.5	80.6±0.9	91.5±1.1	51.7±0.6	61.7±1.5	57.5±0.4	31.5±0.2
	LoRSU	76.2±1.0	53.6±1.1	82.5±1.2	60.8±0.8	82.9±1.0	91.5±0.9	51.6±0.9	61.3±0.7	57.7±0.4	31.9±0.4
CL-20	LN	74.5±0.5	52.6±0.7	82.5±0.5	58.8±0.7	77.0±0.4	92.4±0.5	51.9±1.0	62.5±0.5	58.0±0.3	31.2±0.1
	F-FT	66.5±0.8	51.1±0.7	79.1±0.4	56.7±0.6	51.2±0.7	92.0±0.4	51.6±0.6	61.4±0.8	60.1±0.1	31.5±0.2
	F-EWC	69.3±0.3	51.2±1.0	60.5±0.8	57.1±0.6	54.1±0.6	89.7±0.6	51.9±0.6	60.9±0.7	58.4±0.2	31.8±0.2
	LoRA	71.1±0.7	50.9±0.5	80.3±1.0	59.4±0.7	64.6±0.7	91.1±0.7	52.0±0.4	62.3±0.6	62.3±0.2	31.3±0.1
	AdaLoRA	70.0±0.6	47.3±0.8	78.4±0.9	51.7±0.4	69.3±0.5	91.3±0.7	51.7±0.9	60.8±0.9	58.1±0.2	31.6±0.1
	SPU	75.6±0.9	53.1±0.3	82.8±0.9	59.9±0.8	81.5±0.6	92.3±0.4	51.9±0.5	61.5±0.8	58.8±0.2	31.7±0.1
	LoRSU	75.3±1.0	53.7±0.8	82.8±0.4	60.7±0.8	82.7±0.7	91.6±0.6	51.6±0.4	61.5±0.4	58.4±0.2	31.4±0.2
	LN	73.1±0.3	53.0±0.2	82.0±0.1	59.1±0.2	80.7±0.0	92.4±0.2	51.8±0.3	62.0±0.1	60.4±0.0	32.0±0.0
CL-50	F-FT	58.0±0.4	50.3±0.0	76.8±0.1	57.2±0.2	34.7±0.1	89.7±0.0	51.7±0.2	61.6±0.2	58.1±0.0	31.6±0.1
	F-EWC	59.0±0.1	64.5±0.1	77.2±0.1	56.3±0.1	38.0±0.2	87.3±0.2	51.9±0.2	60.7±0.2	58.2±0.1	31.8±0.0
	LoRA	62.8±0.3	47.2±0.4	72.4±0.4	54.4±0.2	61.6±0.4	90.2±0.3	51.7±0.2	62.0±0.1	60.8±0.0	30.9±0.1
	AdaLoRA	67.2±0.2	49.3±0.3	78.8±0.3	56.9±0.3	58.8±0.3	89.6±0.3	51.8±0.1	61.9±0.2	56.0±0.1	31.6±0.0
	SPU	75.1±0.3	53.4±0.2	82.5±0.2	60.2±0.3	81.9±0.1	92.3±0.3	51.8±0.1	61.6±0.1	57.1±0.1	31.9±0.0
	LoRSU	75.4±0.3	53.9±0.1	83.1±0.2	60.3±0.1	83.1±0.1	92.1±0.1	51.6±0.2	61.2±0.0	57.6±0.0	31.1±0.0

Table 13. Average accuracy (ACC) and backward transfer (BWT) scores (%) for LLaVA with the fine-tuned CLIP-L-14. Each column indicates the setting and fine-tuning method. We include error bars over 3 runs.

Setting	FT Dataset	FT Method									
		Zr-Shot		LoRA		SPU		LoRSU			
		ACC (↑)	BWT (↑)	ACC (↑)	BWT (↑)	ACC (↑)	BWT (↑)	ACC (↑)	BWT (↑)	ACC (↑)	BWT (↑)
CL-5	GTS	75.4	0.0	79.2±0.7	-7.1±0.8	80.8±0.5	0.5±0.6	81.1±0.6	0.4±0.7		
	TSI	54.0	0.0	55.5±0.9	-2.5±0.6	55.5±0.6	0.2±0.5	57.0±0.8	0.5±0.6		
	AIR	60.4	0.0	59.2±0.8	-2.1±0.7	64.7±0.5	2.8±0.6	65.0±0.7	2.5±0.6		
	ESAT	76.4	0.0	73.8±0.9	-3.4±0.6	79.8±0.6	1.5±0.7	82.2±0.7	2.0±0.6		
CL-20	GTS	75.4	0.0	77.2±0.4	-9.1±0.5	82.8±0.4	-0.6±0.3	83.5±0.6	-0.4±0.3		
	TSI	54.0	0.0	60.6±0.3	-7.2±0.4	60.1±0.5	-1.7±0.3	62.1±0.3	-0.9±0.4		
	AIR	60.4	0.0	64.3±0.4	-3.6±0.6	65.2±0.7	1.1±0.4	65.4±0.3	0.9±0.4		
	ESAT	76.4	0.0	64.1±0.5	-18.3±0.7	82.0±0.4	2.0±0.2	82.7±0.5	0.1±0.3		
CL-50	GTS	75.4	0.0	79.3±0.3	-10.3±0.5	83.8±0.2	-0.7±0.1	84.7±0.3	-0.5±0.2		
	TSI	54.0	0.0	67.0±0.3	-8.1±0.6	61.8±0.2	-1.9±0.3	67.9±0.2	-1.1±0.3		
	AIR	60.4	0.0	65.6±0.4	-6.1±0.3	67.1±0.3	0.5±0.2	67.7±0.3	0.7±0.3		
	ESAT	76.4	0.0	61.4±0.3	-27.8±0.4	81.2±0.3	-2.4±0.2	82.1±0.4	-0.8±0.2		

Table 14. Exact accuracy scores (%) for each baseline used to fine-tune the model on the *GTS* dataset under three different continual learning (5, 10, 50 shots) settings. We include error bars over 3 runs.

Setting	PEFT Method	VQA Datasets (Acc %)									
		GTS	TSI	CAn	AIR	ESAT	DALLE	VSR	HM	MMVP	VisOnly
CL-5	Zr-Shot	75.6	53.1	82.7	60.4	76.1	91.1	51.5	61.2	58.0	31.3
	LoRA-L	71.5 \pm 1.2	52.3 \pm 0.5	81.2 \pm 0.6	60.0 \pm 1.2	75.5 \pm 0.9	91.5 \pm 1.3	51.9 \pm 1.5	61.2 \pm 1.1	57.6 \pm 0.3	32.2 \pm 0.5
	LoRA	76.3 \pm 0.8	52.6 \pm 1.4	73.3 \pm 0.6	56.7 \pm 1.2	49.3 \pm 0.8	87.1 \pm 1.3	51.8 \pm 1.2	61.3 \pm 1.2	58.1 \pm 0.3	31.6 \pm 0.4
	LoRSU	82.0 \pm 1.3	53.5 \pm 1.3	82.4 \pm 0.8	60.8 \pm 1.4	66.6 \pm 0.9	91.5 \pm 1.4	51.6 \pm 0.7	61.7 \pm 1.4	59.8 \pm 0.2	31.6 \pm 0.2
	LoRA-Ppl	68.1 \pm 0.8	54.5 \pm 1.4	80.7 \pm 0.6	59.3 \pm 1.2	52.8 \pm 0.8	90.7 \pm 1.3	51.7 \pm 1.2	60.7 \pm 1.2	54.8 \pm 0.4	33.4 \pm 0.5
	LoRA-F	72.9 \pm 0.9	54.0 \pm 0.7	81.5 \pm 0.9	59.6 \pm 0.8	61.9 \pm 0.8	90.3 \pm 1.1	51.9 \pm 0.8	60.9 \pm 1.2	58.4 \pm 0.4	31.1 \pm 0.3
CL-20	LoRSU-Ppl	77.2 \pm 1.4	55.1 \pm 1.5	82.1 \pm 0.7	58.9 \pm 1.0	67.0 \pm 0.6	90.9 \pm 1.3	51.8 \pm 0.6	61.6 \pm 1.3	58.7 \pm 0.3	30.4 \pm 0.3
	LoRA-L	74.2 \pm 0.9	52.2 \pm 0.9	82.1 \pm 0.5	59.6 \pm 1.0	75.9 \pm 0.6	91.8 \pm 1.0	51.6 \pm 0.4	62.1 \pm 0.9	59.1 \pm 0.2	31.8 \pm 0.2
	LoRA	78.1 \pm 0.8	55.6 \pm 0.3	59.0 \pm 0.9	47.6 \pm 0.4	26.0 \pm 0.6	83.6 \pm 0.8	52.1 \pm 0.5	62.1 \pm 1.0	53.7 \pm 0.3	30.8 \pm 0.2
	LoRSU	84.2 \pm 0.9	52.9 \pm 0.6	82.2 \pm 0.5	60.7 \pm 0.6	64.7 \pm 0.6	90.8 \pm 0.5	51.9 \pm 0.4	61.7 \pm 0.5	59.5 \pm 0.1	31.6 \pm 0.2
	LoRA-Ppl	75.1 \pm 0.9	50.4 \pm 0.9	75.8 \pm 0.4	56.5 \pm 0.3	40.1 \pm 0.9	89.7 \pm 0.8	51.6 \pm 0.7	57.8 \pm 0.8	54.2 \pm 0.2	31.5 \pm 0.4
	LoRA-F	74.2 \pm 0.8	52.7 \pm 0.3	80.1 \pm 0.9	59.5 \pm 0.4	66.0 \pm 0.6	90.1 \pm 0.8	52.1 \pm 0.5	64.7 \pm 1.0	60.4 \pm 0.4	32.3 \pm 0.2
CL-50	LoRSU-Ppl	79.5 \pm 0.8	56.1 \pm 0.5	82.1 \pm 0.9	59.8 \pm 0.4	66.1 \pm 0.4	90.8 \pm 1.0	51.7 \pm 0.5	62.1 \pm 0.6	59.0 \pm 0.3	31.5 \pm 0.3
	LoRA-L	74.9 \pm 0.2	51.7 \pm 0.2	81.8 \pm 0.2	59.8 \pm 0.3	75.8 \pm 0.1	91.5 \pm 0.0	52.0 \pm 0.1	61.1 \pm 0.2	57.4 \pm 0.1	31.8 \pm 0.1
	LoRA	78.7 \pm 0.0	50.7 \pm 0.0	62.1 \pm 0.2	47.4 \pm 0.1	24.2 \pm 0.2	82.9 \pm 0.3	51.7 \pm 0.3	61.0 \pm 0.2	54.3 \pm 0.1	30.8 \pm 0.0
	LoRSU	85.3 \pm 0.1	54.2 \pm 0.1	81.9 \pm 0.2	60.5 \pm 0.2	61.4 \pm 0.3	91.0 \pm 0.1	51.7 \pm 0.2	62.2 \pm 0.4	58.9 \pm 0.1	31.8 \pm 0.1
	LoRA-Ppl	74.2 \pm 0.1	49.4 \pm 0.2	76.0 \pm 0.2	57.9 \pm 0.3	37.2 \pm 0.0	89.5 \pm 0.2	51.7 \pm 0.1	57.7 \pm 0.1	55.6 \pm 0.1	29.8 \pm 0.1
	LoRA-F	71.7 \pm 0.2	51.7 \pm 0.4	80.8 \pm 0.4	58.3 \pm 0.0	60.9 \pm 0.3	90.8 \pm 0.1	52.1 \pm 0.0	63.3 \pm 0.1	57.5 \pm 0.0	30.9 \pm 0.1
CL-50	LoRSU-Ppl	82.5 \pm 0.0	55.8 \pm 0.0	82.1 \pm 0.2	59.9 \pm 0.1	65.4 \pm 0.2	91.0 \pm 0.3	51.6 \pm 0.3	61.7 \pm 0.2	62.3 \pm 0.1	32.2 \pm 0.0

D.3. CLIP-based vs. Perplexity-based Updates+

The detailed accuracies for all baselines and datasets used to create Table 3 of the main paper can be found in Tables 14 through 18. We have also included results on fine-tuning the model using *MMVP* dataset in Table 21.

E. Extra Ablation Studies

E.1. Ablation on the rank r of LoRSU

In Table 23, we investigate the effect on performance of using different ranks for LoRSU. As the rank r increases, the VQA accuracy on the target dataset slightly improves, peaking at $r = 64$. Beyond that, performance slightly decreases. Performance on other datasets remains relatively stable with small fluctuations.

E.2. Ablation on the number of optimal attention heads of LoRSU

In Table 24, we examine how the number of attention heads chosen to be fine-tuned affects LoRSU’s performance. We notice that more attention heads marginally improve the performance of the model while the extra flexibility can cause more forgetting, e.g. ESAT.

E.3. Robustness on the Choice of Attention Heads

We show in Table 25 that LoRSU’s mechanism of choosing the most important attention heads provides a clear advantage in terms of robustness over the other two LoRSU’s variants, LoRSU-Rand and LoRSU-AAH. We can see that TI and CC decline in a lower rate compared to that of LoRSU-RAnd and LoRSU-AAH, as we increase the number of training epochs.. As expected, LoRSU-Rand appears to be the least robust method since the random choice of the attention heads constitute it more unstable.

Table 15. Exact accuracy scores (%) for each baseline used to fine-tune the model on the *TSI* dataset under three different continual learning (5, 10, 50 shots) settings. We include error bars over 3 runs.

		VQA Datasets (Acc %)									
Setting	PEFT Method	GTS	TSI	CAn	AIR	ESAT	DALLE	VSR	HM	MMVP	VisOnly
CL-5	Zr-Shot	75.6	53.1	82.7	60.4	76.1	91.1	51.5	61.2	58.0	31.3
	LoRA-L	76.0±1.5	59.1±0.6	82.7±0.9	60.7±0.7	75.9±0.9	91.5±1.0	51.5±0.9	63.6±1.2	54.1±0.4	31.2±0.4
	LoRA	73.4±1.0	53.0±0.9	80.2±0.6	58.8±0.7	59.1±1.4	90.2±1.1	51.6±1.3	61.2±1.4	56.7±0.4	31.7±0.4
	LoRSU	75.9±0.9	56.3±0.7	82.7±0.9	60.8±1.0	76.2±1.4	91.3±1.2	51.6±0.9	61.7±0.8	57.7±0.3	31.2±0.3
	LoRA-Ppl	75.0±1.0	64.0±0.6	82.8±1.3	58.4±1.0	60.8±0.8	88.7±1.3	51.6±1.4	61.5±1.0	55.0±0.4	32.2±0.4
	LoRA-F	75.3±0.5	45.1±1.1	82.5±0.9	57.2±1.5	73.2±1.0	83.9±1.2	53.8±0.9	64.3±1.3	45.6±0.3	30.9±0.4
CL-20	LoRSU-Ppl	76.1±1.1	66.2±1.0	83.9±1.1	66.1±0.9	76.1±1.2	91.1±1.4	52.0±0.9	64.4±1.4	60.8±0.5	31.1±0.4
	LoRA-L	76.1±0.7	59.0±0.6	82.4±0.4	60.8±0.4	75.7±0.9	91.3±0.7	51.5±0.9	63.9±1.0	55.4±0.3	30.8±0.3
	LoRA	68.5±0.7	61.6±0.3	76.7±0.9	55.3±0.7	55.6±0.6	88.8±0.8	51.9±0.3	61.4±0.6	59.1±0.3	31.1±0.3
	LoRSU	75.9±0.6	63.7±0.4	82.8±0.8	60.4±0.3	73.4±0.6	90.9±0.6	51.7±0.4	61.5±0.7	58.8±0.2	31.9±0.2
	LoRA-Ppl	62.1±0.6	59.6±0.5	71.9±0.6	48.3±0.7	42.5±1.0	75.8±0.8	51.6±0.6	49.0±0.5	49.7±0.3	32.4±0.2
	LoRA-F	76.1±0.5	56.0±0.5	82.8±0.9	58.2±0.4	67.7±0.9	87.5±0.8	51.6±0.8	64.4±0.5	40.3±0.4	31.2±0.2
CL-50	LoRSU-Ppl	76.4±0.7	67.0±0.4	83.0±0.7	57.4±0.4	74.0±0.8	88.1±0.3	51.8±0.6	63.6±0.5	57.6±0.2	30.8±0.3
	LoRA-L	76.4±0.2	63.0±0.2	81.9±0.2	60.5±0.2	75.6±0.2	91.1±0.2	51.7±0.2	64.1±0.3	55.6±0.2	30.9±0.0
	LoRA	66.1±0.2	71.3±0.3	76.0±0.1	56.0±0.1	44.5±0.2	88.9±0.3	51.8±0.1	60.4±0.2	56.3±0.1	31.6±0.1
	LoRSU	75.3±0.2	72.2±0.4	82.4±0.3	59.7±0.3	72.5±0.3	90.8±0.3	51.7±0.2	61.7±0.4	58.5±0.1	31.7±0.0
	LoRA-Ppl	46.3±0.3	51.5±0.3	63.4±0.1	40.1±0.1	41.3±0.4	73.9±0.2	51.7±0.3	49.5±0.3	40.2±0.1	32.7±0.1
	LoRA-F	74.0±0.2	68.2±0.1	81.6±0.3	59.2±0.0	75.1±0.2	88.5±0.2	56.8±0.1	65.0±0.3	50.8±0.1	30.4±0.1
	LoRSU-Ppl	75.8±0.2	75.1±0.2	82.1±0.3	56.0±0.4	74.2±0.4	86.0±0.4	52.0±0.0	63.2±0.0	58.1±0.1	30.2±0.1

Table 16. Exact accuracy scores (%) for each baseline used to fine-tune the model on the *CAn* dataset under three different continual learning (5, 10, 50 shots) settings. We include error bars over 3 runs.

		VQA Datasets (Acc %)									
Setting	PEFT Method	GTS	TSI	CAn	AIR	ESAT	DALLE	VSR	HM	MMVP	VisOnly
CL-5	Zr-Shot	75.6	53.1	82.7	60.4	76.1	91.1	51.5	61.2	58.0	31.3
	LoRA-L	75.5±1.4	53.1±0.8	79.4±1.4	59.2±0.6	75.2±0.9	91.5±1.1	52.4±1.3	60.2±1.1	57.7±0.5	32.1±0.3
	LoRA	69.7±1.4	44.8±1.1	81.4±0.7	56.9±1.0	50.7±1.3	92.9±1.3	52.0±1.0	61.8±1.5	56.5±0.4	31.3±0.4
	LoRSU	75.2±0.8	52.7±0.9	83.0±1.0	60.1±0.7	76.8±1.0	91.8±1.4	51.6±1.1	62.3±1.2	58.7±0.3	31.4±0.4
	LoRA-Ppl	65.8±1.1	50.7±0.6	79.2±0.5	48.4±1.4	63.0±1.2	86.7±1.3	51.8±1.0	57.2±1.4	52.5±0.3	32.4±0.4
	LoRA-F	70.1±0.6	52.2±0.7	78.6±0.7	50.9±0.9	73.4±0.8	91.3±1.0	54.7±0.8	62.2±1.4	58.0±0.5	31.3±0.3
CL-20	LoRSU-Ppl	74.6±0.9	51.3±1.4	82.9±1.2	58.4±1.2	77.7±1.2	91.8±1.3	51.5±1.1	64.7±1.4	56.5±0.6	29.8±0.3
	LoRA-L	73.6±1.0	52.2±0.9	80.8±0.9	56.7±0.4	74.7±0.8	91.7±0.5	52.2±0.6	60.9±0.8	59.1±0.3	31.9±0.4
	LoRA	67.5±0.6	48.9±0.6	80.4±0.4	57.3±0.9	39.7±0.4	91.1±0.6	51.8±0.9	61.7±0.3	60.1±0.2	31.9±0.3
	LoRSU	75.3±0.8	53.1±0.9	83.8±0.9	58.8±1.0	75.5±0.7	92.0±0.3	51.9±0.4	62.3±0.6	60.4±0.2	31.6±0.2
	LoRA-Ppl	65.6±0.9	47.0±0.7	79.0±0.4	46.0±0.6	58.9±0.8	82.5±0.8	51.9±0.7	43.9±1.0	52.5±0.4	30.4±0.3
	LoRA-F	69.4±0.9	54.9±0.4	80.6±0.4	50.4±0.5	72.0±0.8	91.2±0.5	51.9±0.9	64.3±1.0	57.0±0.3	31.6±0.3
CL-50	LoRSU-Ppl	72.4±0.6	49.2±0.4	83.2±0.7	56.4±0.9	75.5±0.6	91.8±0.9	51.6±0.5	61.0±0.8	57.7±0.3	31.6±0.3
	LoRA-L	73.8±0.1	51.6±0.2	80.9±0.2	56.9±0.1	74.9±0.2	91.3±0.3	51.7±0.2	61.2±0.3	58.0±0.1	32.4±0.1
	LoRA	66.8±0.2	47.8±0.3	82.3±0.2	55.7±0.0	52.0±0.3	91.0±0.3	51.7±0.3	61.6±0.2	60.2±0.0	31.6±0.1
	LoRSU	75.0±0.2	51.8±0.1	84.0±0.4	58.5±0.2	72.7±0.3	91.9±0.3	51.7±0.1	62.3±0.4	58.1±0.0	31.7±0.1
	LoRA-Ppl	56.2±0.4	36.4±0.0	80.9±0.1	48.5±0.3	54.1±0.3	78.1±0.2	53.6±0.4	62.3±0.3	48.4±0.1	32.4±0.1
	LoRA-F	69.2±0.2	52.0±0.2	80.6±0.1	53.7±0.3	74.4±0.1	90.7±0.2	51.8±0.4	66.5±0.0	58.7±0.1	31.4±0.1
	LoRSU-Ppl	74.9±0.4	49.7±0.4	83.7±0.0	42.5±0.4	74.9±0.2	91.2±0.3	51.2±0.3	52.2±0.4	58.5±0.2	32.3±0.2

Table 17. Exact accuracy scores (%) for each baseline used to fine-tune the model on the *AIR* dataset under three different continual learning (5, 10, 50 shots) settings. We include error bars over 3 runs.

		VQA Datasets (Acc %)									
Setting	PEFT Method	GTS	TSI	CAn	AIR	ESAT	DALLE	VSR	HM	MMVP	VisOnly
CL-5	Zr-Shot	75.6	53.1	82.7	60.4	76.1	91.1	51.5	61.2	58.0	31.3
	LoRA-L	75.6 \pm 0.7	54.4 \pm 0.5	81.8 \pm 1.1	58.7 \pm 0.9	75.7 \pm 1.4	92.0 \pm 1.4	51.6 \pm 0.9	61.0 \pm 0.6	59.1 \pm 0.3	32.2 \pm 0.5
	LoRA	70.9 \pm 0.9	52.7 \pm 0.6	79.0 \pm 0.7	61.7 \pm 0.5	48.8 \pm 0.7	90.6 \pm 0.6	52.0 \pm 0.9	62.5 \pm 0.8	60.0 \pm 0.3	31.1 \pm 0.2
	LoRSU	76.2 \pm 0.8	53.4 \pm 1.4	82.5 \pm 1.0	65.2 \pm 1.3	76.0 \pm 0.9	91.8 \pm 0.8	51.6 \pm 0.8	62.1 \pm 1.1	59.0 \pm 0.4	31.2 \pm 0.3
	LoRA-Ppl	74.9 \pm 0.8	54.2 \pm 1.2	79.1 \pm 0.5	59.7 \pm 0.9	68.5 \pm 0.9	90.8 \pm 1.3	51.8 \pm 0.7	62.0 \pm 0.7	55.1 \pm 0.5	31.1 \pm 0.5
	LoRA-F	72.3 \pm 0.5	50.6 \pm 1.3	78.7 \pm 1.4	70.0 \pm 1.3	64.4 \pm 0.9	90.9 \pm 0.6	54.9 \pm 1.3	57.7 \pm 1.1	62.0 \pm 0.6	32.2 \pm 0.5
CL-20	LoRSU-Ppl	75.6 \pm 1.0	54.6 \pm 1.2	79.8 \pm 1.0	66.2 \pm 0.5	76.4 \pm 1.1	90.6 \pm 1.3	51.7 \pm 1.3	60.1 \pm 0.9	58.8 \pm 0.4	31.1 \pm 0.4
	LoRA-L	75.4 \pm 0.3	53.6 \pm 0.4	82.2 \pm 1.0	64.1 \pm 1.0	75.7 \pm 0.5	92.2 \pm 0.3	51.5 \pm 0.5	61.5 \pm 0.8	58.9 \pm 0.2	31.9 \pm 0.3
	LoRA	71.8 \pm 0.9	51.1 \pm 0.8	78.6 \pm 0.3	65.7 \pm 0.4	63.4 \pm 0.8	89.9 \pm 1.0	51.7 \pm 0.3	62.3 \pm 0.3	56.2 \pm 0.2	31.5 \pm 0.2
	LoRSU	75.7 \pm 0.9	52.6 \pm 0.9	81.4 \pm 0.7	66.3 \pm 0.7	73.0 \pm 0.8	90.9 \pm 0.8	51.9 \pm 0.8	61.8 \pm 0.8	56.9 \pm 0.1	31.6 \pm 0.3
	LoRA-Ppl	72.1 \pm 0.5	48.0 \pm 0.8	72.7 \pm 0.4	65.2 \pm 1.0	65.1 \pm 0.5	90.4 \pm 0.3	51.8 \pm 0.6	61.5 \pm 0.8	55.8 \pm 0.1	31.7 \pm 0.1
	LoRA-F	74.5 \pm 0.8	53.0 \pm 0.3	82.0 \pm 0.6	76.7 \pm 0.6	74.9 \pm 0.9	91.1 \pm 0.3	52.4 \pm 0.6	59.3 \pm 0.8	59.6 \pm 0.4	31.3 \pm 0.3
CL-50	LoRSU-Ppl	76.1 \pm 0.8	55.5 \pm 0.5	78.7 \pm 0.8	66.4 \pm 0.6	75.7 \pm 0.6	91.6 \pm 1.0	51.5 \pm 0.3	59.8 \pm 0.5	58.1 \pm 0.4	31.2 \pm 0.4
	LoRA-L	75.6 \pm 0.2	53.8 \pm 0.1	83.5 \pm 0.1	65.0 \pm 0.0	75.7 \pm 0.1	92.0 \pm 0.0	51.8 \pm 0.2	61.1 \pm 0.1	58.7 \pm 0.1	32.3 \pm 0.0
	LoRA	69.8 \pm 0.0	54.7 \pm 0.0	77.0 \pm 0.3	68.2 \pm 0.3	51.6 \pm 0.1	90.0 \pm 0.1	52.0 \pm 0.4	62.4 \pm 0.0	57.1 \pm 0.1	31.5 \pm 0.1
	LoRSU	75.4 \pm 0.4	52.7 \pm 0.3	81.6 \pm 0.2	68.6 \pm 0.3	69.7 \pm 0.3	91.5 \pm 0.2	51.7 \pm 0.4	62.2 \pm 0.1	58.7 \pm 0.1	31.1 \pm 0.1
	LoRA-Ppl	74.4 \pm 0.1	50.9 \pm 0.4	76.8 \pm 0.2	66.6 \pm 0.3	65.4 \pm 0.2	91.3 \pm 0.1	51.6 \pm 0.1	57.2 \pm 0.2	53.7 \pm 0.1	31.5 \pm 0.1
	LoRA-F	74.6 \pm 0.3	53.2 \pm 0.2	80.7 \pm 0.4	78.3 \pm 0.1	71.4 \pm 0.2	91.4 \pm 0.0	52.9 \pm 0.4	60.0 \pm 0.2	57.4 \pm 0.0	31.1 \pm 0.2
CL-50	LoRSU-Ppl	75.1 \pm 0.2	54.5 \pm 0.1	78.0 \pm 0.4	69.3 \pm 0.1	75.7 \pm 0.1	91.5 \pm 0.1	51.7 \pm 0.0	61.5 \pm 0.1	58.2 \pm 0.0	30.8 \pm 0.0

Table 18. Exact accuracy scores (%) for each baseline used to fine-tune the model on the *ESAT* dataset under three different continual learning (5, 10, 50 shots) settings. We include error bars over 3 runs.

		VQA Datasets (Acc %)									
Setting	PEFT Method	GTS	TSI	CAn	AIR	ESAT	DALLE	VSR	HM	MMVP	VisOnly
CL-5	Zr-Shot	75.6	53.1	82.7	60.4	76.1	91.1	51.5	61.2	58.0	31.3
	LoRA-L	75.4 \pm 0.7	52.2 \pm 1.4	82.8 \pm 0.6	60.6 \pm 1.5	75.9 \pm 1.1	91.7 \pm 0.9	51.5 \pm 0.6	60.2 \pm 0.8	57.6 \pm 0.5	31.6 \pm 0.4
	LoRA	73.2 \pm 1.3	49.3 \pm 1.2	80.6 \pm 0.9	60.4 \pm 1.1	74.5 \pm 0.8	92.3 \pm 1.3	52.0 \pm 1.1	61.6 \pm 1.1	57.4 \pm 0.4	31.4 \pm 0.3
	LoRSU	76.2 \pm 1.0	53.6 \pm 1.1	82.5 \pm 1.2	60.8 \pm 0.8	82.9 \pm 1.0	91.5 \pm 0.9	51.6 \pm 0.9	61.3 \pm 0.7	57.7 \pm 0.4	31.9 \pm 0.4
	LoRA-Ppl	76.0 \pm 0.7	52.6 \pm 1.0	82.6 \pm 1.3	60.4 \pm 1.4	75.5 \pm 0.9	91.9 \pm 1.0	51.8 \pm 0.9	62.8 \pm 0.8	59.0 \pm 0.4	31.6 \pm 0.5
	LoRA-F	74.3 \pm 1.3	51.5 \pm 1.4	81.1 \pm 1.0	60.3 \pm 1.1	81.5 \pm 1.2	90.8 \pm 1.2	51.9 \pm 1.2	61.9 \pm 1.2	57.7 \pm 0.2	31.3 \pm 0.5
CL-20	LoRSU-Ppl	75.6 \pm 1.4	52.3 \pm 0.6	82.0 \pm 1.2	60.5 \pm 1.0	79.8 \pm 1.1	92.3 \pm 0.5	51.8 \pm 1.2	62.2 \pm 1.4	57.7 \pm 0.4	31.3 \pm 0.4
	LoRA-L	75.9 \pm 0.8	52.4 \pm 0.9	82.7 \pm 0.7	60.8 \pm 1.0	76.8 \pm 0.3	91.3 \pm 0.5	51.7 \pm 0.5	60.4 \pm 0.9	61.5 \pm 0.3	31.6 \pm 0.3
	LoRA	71.1 \pm 0.7	50.9 \pm 0.5	80.3 \pm 1.0	59.4 \pm 0.7	64.6 \pm 0.7	91.1 \pm 0.7	52.0 \pm 0.4	62.3 \pm 0.6	62.3 \pm 0.2	31.3 \pm 0.1
	LoRSU	75.3 \pm 1.0	53.7 \pm 0.8	82.8 \pm 0.4	60.7 \pm 0.8	82.7 \pm 0.7	91.6 \pm 0.6	51.6 \pm 0.4	61.5 \pm 0.4	58.4 \pm 0.2	31.4 \pm 0.2
	LoRA-Ppl	75.5 \pm 0.9	51.6 \pm 0.7	82.0 \pm 0.4	59.3 \pm 0.6	74.9 \pm 0.3	91.6 \pm 0.5	51.7 \pm 0.6	62.8 \pm 0.5	57.0 \pm 0.1	32.1 \pm 0.1
	LoRA-F	74.8 \pm 0.7	52.7 \pm 1.0	81.6 \pm 0.8	59.4 \pm 0.9	71.5 \pm 0.7	91.0 \pm 0.8	51.7 \pm 0.7	63.4 \pm 0.8	58.9 \pm 0.2	31.0 \pm 0.2
CL-50	LoRSU-Ppl	74.1 \pm 1.0	52.0 \pm 0.9	82.5 \pm 0.7	59.8 \pm 0.8	79.0 \pm 0.7	92.1 \pm 0.7	51.8 \pm 0.9	61.8 \pm 0.4	58.7 \pm 0.4	31.6 \pm 0.3
	LoRA-L	75.6 \pm 0.2	53.0 \pm 0.1	82.7 \pm 0.3	60.6 \pm 0.3	77.1 \pm 0.2	91.5 \pm 0.2	51.7 \pm 0.1	60.7 \pm 0.0	59.8 \pm 0.1	31.4 \pm 0.1
	LoRA	62.8 \pm 0.3	47.2 \pm 0.4	72.4 \pm 0.4	54.4 \pm 0.2	61.6 \pm 0.4	90.2 \pm 0.3	51.7 \pm 0.2	62.0 \pm 0.1	60.8 \pm 0.0	30.9 \pm 0.1
	LoRSU	75.4 \pm 0.3	53.9 \pm 0.1	83.1 \pm 0.2	60.3 \pm 0.1	83.1 \pm 0.1	92.1 \pm 0.1	51.6 \pm 0.2	61.2 \pm 0.0	57.6 \pm 0.0	31.1 \pm 0.0
	LoRA-Ppl	74.9 \pm 0.3	51.7 \pm 0.3	81.9 \pm 0.2	59.8 \pm 0.2	77.8 \pm 0.1	92.1 \pm 0.3	51.8 \pm 0.2	62.9 \pm 0.3	59.4 \pm 0.2	31.9 \pm 0.1
	LoRA-F	73.6 \pm 0.0	51.8 \pm 0.3	81.2 \pm 0.0	58.1 \pm 0.1	66.6 \pm 0.3	90.7 \pm 0.1	51.6 \pm 0.1	63.7 \pm 0.3	58.4 \pm 0.1	30.5 \pm 0.0
CL-50	LoRSU-Ppl	72.9 \pm 0.1	51.1 \pm 0.3	81.3 \pm 0.4	59.4 \pm 0.4	75.4 \pm 0.2	91.6 \pm 0.2	51.7 \pm 0.1	62.7 \pm 0.4	57.5 \pm 0.1	32.1 \pm 0.0

Table 19. Exact accuracy scores (%) for each baseline used to fine-tune the model on the *HM* dataset under three different continual learning (5, 10, 50 shots) settings. We include error bars over 3 runs.

		VQA Datasets (Acc %)									
Setting	PEFT Method	GTS	TSI	CAn	AIR	ESAT	DALLE	VSR	HM	MMVP	VisOnly
CL-5	Zr-Shot	75.6	53.1	82.7	60.4	76.1	91.1	51.5	61.2	58.0	31.3
	LoRA-L	76.5±1.0	51.5±1.1	83.2±1.2	60.5±0.8	75.7±1.0	90.9±0.9	51.6±0.9	68.6±0.7	34.4±0.5	31.1±0.5
	LoRA	68.8±0.8	47.0±1.0	70.5±0.8	51.7±1.1	54.1±0.6	89.1±0.8	52.2±1.5	60.8±0.8	54.7±0.6	30.5±0.3
	LoRSU	75.7±1.2	54.1±1.1	82.9±0.6	60.7±1.0	76.3±1.1	92.2±0.6	51.5±0.9	61.8±1.2	58.1±0.2	31.9±0.5
	LoRA-Ppl	76.2±0.6	48.4±1.4	82.5±1.2	57.2±0.9	72.8±0.9	90.9±0.9	51.8±1.0	60.0±1.0	56.4±0.4	33.1±0.4
	LoRA-F	71.8±1.1	47.8±0.8	79.9±1.5	57.6±1.0	63.2±1.1	90.1±1.0	48.0±0.7	67.2±0.9	49.0±0.3	31.5±0.2
CL-20	LoRSU-Ppl	76.6±1.0	51.7±1.3	83.6±1.4	60.3±0.6	75.2±0.8	90.8±1.0	51.7±1.3	60.4±1.4	60.7±0.5	31.2±0.2
	LoRA-L	75.1±0.9	50.5±0.3	82.1±0.9	59.3±0.8	65.1±0.6	91.8±0.4	51.9±0.5	71.8±0.8	52.8±0.3	31.7±0.2
	LoRA	68.1±1.0	46.8±0.8	76.3±0.4	56.4±0.8	49.6±0.7	87.3±0.6	51.7±0.4	59.4±0.4	59.7±0.3	31.4±0.3
	LoRSU	76.1±0.8	53.0±0.7	82.7±0.5	60.4±0.6	75.7±0.4	92.1±0.7	51.8±0.8	61.9±0.5	58.4±0.2	31.5±0.2
	LoRA-Ppl	77.0±0.9	52.0±0.4	83.9±0.5	63.6±0.7	73.4±0.5	90.5±0.3	53.1±0.7	71.9±0.7	54.1±0.2	31.1±0.4
	LoRA-F	75.6±0.4	50.9±0.5	80.6±0.5	60.8±0.5	71.2±0.7	90.9±0.7	52.2±0.7	72.9±0.7	53.6±0.3	31.6±0.1
CL-50	LoRSU-Ppl	76.1±0.8	49.8±0.9	83.5±0.9	59.8±0.6	76.1±0.9	91.0±0.9	51.7±0.6	72.1±0.4	59.5±0.2	30.5±0.4
	LoRA-L	75.8±0.2	49.5±0.3	83.4±0.3	59.9±0.3	71.1±0.3	89.9±0.3	51.7±0.1	71.4±0.2	48.7±0.1	31.1±0.0
	LoRA	72.7±0.3	47.1±0.2	72.6±0.2	56.7±0.3	60.4±0.1	89.7±0.3	51.9±0.1	61.9±0.1	57.1±0.2	31.1±0.0
	LoRSU	75.3±0.3	53.2±0.1	83.3±0.2	60.5±0.1	74.9±0.1	92.2±0.1	51.6±0.2	61.5±0.0	58.9±0.1	31.3±0.0
	LoRA-Ppl	76.6±0.2	49.3±0.4	81.9±0.3	60.3±0.4	72.7±0.2	89.8±0.3	52.5±0.2	73.7±0.3	52.7±0.0	30.9±0.1
	LoRA-F	74.1±0.1	52.0±0.3	80.6±0.2	57.0±0.1	63.5±0.3	88.7±0.1	53.0±0.4	73.5±0.2	46.0±0.1	31.8±0.0
	LoRSU-Ppl	76.0±0.1	50.4±0.1	83.4±0.1	60.6±0.4	76.4±0.1	91.4±0.2	51.9±0.1	73.4±0.4	59.8±0.1	32.0±0.1

Table 20. Exact accuracy scores (%) for each baseline used to fine-tune the model on the *VSR* dataset under three different continual learning (5, 10, 50 shots) settings. We include error bars over 3 runs.

		VQA Datasets (Acc %)									
Setting	PEFT Method	GTS	TSI	CAn	AIR	ESAT	DALLE	VSR	HM	MMVP	VisOnly
CL-5	Zr-Shot	75.6	53.1	82.7	60.4	76.1	91.1	51.5	61.2	58.0	31.3
	LoRA-L	75.3±0.7	59.9±1.4	81.0±1.1	56.2±0.5	66.8±1.3	90.1±1.3	68.3±1.1	65.0±1.4	57.6±0.3	32.5±0.4
	LoRA	72.6±1.3	49.5±1.5	78.2±0.8	57.5±1.5	55.0±0.9	88.8±0.7	52.0±1.0	61.9±1.5	59.7±0.3	30.4±0.5
	LoRSU	75.6±0.7	52.2±1.4	82.2±0.6	60.1±0.9	77.9±0.6	91.1±1.1	51.9±1.3	62.2±1.5	58.4±0.3	31.7±0.3
	LoRA-Ppl	65.8±0.7	48.7±0.8	65.4±1.3	33.8±1.4	48.8±0.5	81.7±1.2	61.7±0.5	56.2±0.7	43.6±0.2	32.8±0.4
	LoRA-F	76.0±0.9	64.5±0.8	81.2±1.3	57.6±0.6	69.7±1.5	89.4±0.8	69.5±1.0	12.8±0.5	30.3±0.5	13.0±0.3
CL-20	LoRSU-Ppl	73.6±0.7	57.5±1.1	80.3±1.1	57.8±1.3	73.1±1.3	90.7±1.1	62.0±1.5	57.4±0.5	57.9±0.6	30.3±0.4
	LoRA-L	77.1±0.8	54.7±0.9	84.5±0.9	61.4±0.5	75.5±0.7	90.9±0.8	73.7±0.5	64.5±0.8	56.9±0.2	32.6±0.4
	LoRA	72.6±0.7	54.5±0.9	76.6±0.8	57.4±0.7	57.3±0.4	87.9±0.8	51.9±0.7	59.0±0.5	57.6±0.2	31.3±0.4
	LoRSU	74.9±0.6	54.6±0.5	82.1±0.8	58.5±0.7	75.5±0.5	91.6±0.5	51.6±0.6	62.4±0.7	57.5±0.2	30.9±0.2
	LoRA-Ppl	74.9±0.4	62.2±0.4	82.4±0.3	58.2±0.7	70.5±0.7	89.0±0.6	71.0±0.8	64.8±0.5	55.8±0.2	28.6±0.2
	LoRA-F	75.4±0.5	60.6±0.5	80.9±0.9	56.6±0.9	63.1±0.7	88.2±0.6	74.8±0.5	48.7±0.9	50.1±0.4	20.2±0.2
CL-50	LoRSU-Ppl	72.6±0.8	52.7±0.5	81.6±0.8	60.3±0.5	69.4±0.7	89.6±0.5	74.4±0.9	62.5±0.8	57.1±0.3	29.7±0.4
	LoRA-L	77.2±0.3	56.5±0.1	84.5±0.0	61.4±0.2	76.4±0.2	91.5±0.3	73.4±0.1	65.3±0.2	54.4±0.1	31.5±0.1
	LoRA	73.4±0.1	53.8±0.0	74.6±0.4	56.7±0.1	56.2±0.1	87.0±0.2	51.9±0.0	59.2±0.2	57.6±0.1	30.8±0.0
	LoRSU	75.3±0.1	54.7±0.1	81.6±0.1	58.3±0.2	75.7±0.1	91.4±0.4	53.8±0.2	62.1±0.3	57.3±0.1	30.8±0.0
	LoRA-Ppl	71.7±0.1	48.7±0.1	75.1±0.2	46.3±0.4	64.6±0.3	87.9±0.2	71.7±0.4	61.9±0.2	55.1±0.1	30.9±0.0
	LoRA-F	76.3±0.3	64.2±0.2	84.5±0.4	58.1±0.3	69.6±0.1	90.1±0.1	72.5±0.3	64.6±0.1	61.4±0.1	30.6±0.1
	LoRSU-Ppl	72.1±0.2	49.8±0.1	74.8±0.3	57.6±0.0	71.0±0.4	88.2±0.1	74.9±0.1	58.3±0.2	55.4±0.2	30.0±0.2

Table 21. Exact accuracy scores (%) for each baseline used to fine-tune the model on the *MMVP* dataset under three different continual learning (5, 10, 50 shots) settings. We include error bars over 3 runs.

VQA Datasets (Acc %)											
Setting	PEFT Method	GTS	TSI	CAn	AIR	ESAT	DALLE	VSR	HM	MMVP	VisOnly
CL	Zr-Shot	75.6	53.1	82.7	60.4	76.1	91.1	51.5	61.2	58.0	31.3
	LoRA-L	75.5	52.8	82.0	60.5	76.0	91.5	51.5	63.6	57.7	30.6
	LoRA-Ppl	75.5	53.6	83.0	60.3	75.6	91.1	51.5	63.1	60.7	31.7
	LoRA-F	75.2	52.9	81.3	60.5	74.3	90.4	51.6	63.6	60.0	31.4
	LoRSU-Ppl	75.1	52.0	81.2	57.4	75.2	90.2	51.7	63.9	60.3	30.8

Table 22. Exact accuracy scores (%) for each baseline used to fine-tune the model on the *VisOnly* dataset under three different continual learning (5, 10, 50 shots) settings. We include error bars over 3 runs.

VQA Datasets (Acc %)											
Setting	PEFT Method	GTS	TSI	CAn	AIR	ESAT	DALLE	VSR	HM	MMVP	VisOnly
CL-5	Zr-Shot	75.6	53.1	82.7	60.4	76.1	91.1	51.5	61.2	58.0	31.3
	LoRA-L	76.5±1.2	51.9±0.7	82.4±1.4	60.5±1.5	76.1±1.0	91.5±0.6	51.6±0.9	60.3±1.0	57.6±0.3	31.3±0.4
	LoRA	70.9±1.4	52.1±1.2	77.5±1.3	55.6±0.6	52.6±0.8	89.3±0.6	51.7±0.8	61.7±0.7	56.9±0.6	30.9±0.5
	LoRSU	75.9±0.7	53.1±0.8	82.5±0.7	60.4±1.0	76.1±1.5	91.9±0.8	51.5±1.3	61.3±1.2	58.9±0.4	31.5±0.2
	LoRA-Ppl	76.3±1.1	50.7±1.1	82.2±0.9	61.0±1.3	73.4±0.9	91.7±1.3	52.1±1.1	59.3±1.3	58.0±0.2	35.0±0.5
	LoRA-F	76.0±0.8	51.1±1.4	82.9±1.1	59.9±0.7	71.2±1.2	91.7±1.1	51.6±1.3	60.8±0.7	58.4±0.2	34.9±0.4
	LoRSU-Ppl	76.2±1.1	53.0±0.9	83.4±0.7	61.3±1.4	76.6±0.8	92.3±0.5	52.0±1.0	61.6±0.7	60.7±0.3	32.0±0.5
CL-20	LoRA-L	77.8±1.0	53.0±0.8	83.4±0.4	62.1±0.6	75.5±0.8	91.6±0.4	52.4±0.9	61.2±0.6	55.6±0.3	32.5±0.3
	LoRA	73.3±0.9	49.3±0.4	77.9±0.6	56.4±0.6	47.7±0.8	91.2±0.6	51.8±0.8	61.5±0.6	57.0±0.3	32.8±0.1
	LoRSU	75.7±0.5	53.3±0.7	82.0±0.5	60.0±0.5	76.1±0.6	91.9±0.9	51.7±0.6	61.6±0.3	58.2±0.3	31.5±0.4
	LoRA-Ppl	78.0±0.4	52.8±0.4	83.7±0.6	60.9±0.7	74.3±0.4	91.5±0.7	51.9±0.5	61.7±0.7	56.0±0.2	32.8±0.3
	LoRA-F	77.4±0.6	51.7±0.9	83.7±0.6	59.7±0.7	73.9±0.9	91.2±0.5	53.4±0.4	62.0±0.9	56.9±0.4	31.0±0.3
	LoRSU-Ppl	76.7±0.5	53.7±0.4	83.8±0.6	61.4±0.3	75.5±0.6	91.2±0.8	51.8±0.3	61.9±0.9	59.6±0.4	31.3±0.2
CL-50	LoRA-L	76.4±0.4	54.5±0.3	84.1±0.3	61.3±0.0	73.9±0.1	91.5±0.1	51.9±0.3	62.8±0.1	55.4±0.0	32.1±0.1
	LoRA	70.0±0.1	46.8±0.0	70.5±0.1	51.0±0.2	50.9±0.0	88.1±0.0	52.0±0.3	61.2±0.3	57.8±0.2	31.7±0.1
	LoRSU	75.6±0.4	53.1±0.1	81.7±0.3	58.2±0.1	75.3±0.2	91.8±0.3	51.7±0.1	62.1±0.1	58.3±0.1	31.9±0.0
	LoRA-Ppl	76.9±0.4	54.6±0.1	84.1±0.3	60.5±0.2	74.9±0.4	91.2±0.3	51.8±0.3	62.5±0.3	56.0±0.1	33.0±0.0
	LoRA-F	77.1±0.0	53.0±0.2	83.9±0.4	60.9±0.1	73.1±0.1	92.2±0.3	51.9±0.2	61.4±0.4	58.0±0.0	32.5±0.1
LoRSU-Ppl	76.1±0.3	51.5±0.2	81.6±0.1	60.2±0.0	75.6±0.2	92.2±0.3	52.0±0.2	61.2±0.3	58.3±0.0	33.5±0.1	

Table 23. Ablation study over the effect of the rank r used by LoRSU to fine-tune the image encoder, CLIP-L-14. We report the VQA accuracies of the last session in the *50-shot* CL setting. The accuracies on the target dataset are in red color. For this experiment, we use two attention heads to fine-tune with LoRSU.

		VQA Datasets (Acc %)									
FT Dataset	rank (r)	GTS	TSI	CAn	AIR	ESAT	DALLE	VSR	HM	MMVP	VisOnly
GTS	8	83.0	53.2	81.3	60.9	61.0	91.2	51.5	61.6	60.0	31.6
	16	83.9	53.4	81.5	60.2	54.0	91.4	51.5	62.1	60.7	31.6
	32	84.8	53.1	81.9	60.5	58.0	90.6	51.6	61.8	58.7	31.5
	64	84.9	53.2	81.3	60.7	61.7	90.9	51.5	61.9	59.3	31.3
	128	84.3	53.2	81.8	60.6	56.8	91.5	51.6	61.8	58.7	31.2
	256	84.5	53.1	81.5	61.1	51.5	90.3	51.6	62.0	58.7	31.6
TSI	8	75.2	67.2	82.0	59.2	71.6	91.1	51.5	61.6	58.0	31.5
	16	75.4	68.0	82.3	59.1	71.0	90.6	51.6	61.6	56.7	31.2
	32	74.9	68.9	81.8	59.3	70.1	91.2	51.5	61.6	58.0	31.6
	64	75.3	72.1	82.0	59.3	72.3	90.5	51.6	61.4	58.0	31.6
	128	75.1	65.8	81.7	59.0	70.0	90.6	51.5	62.1	56.7	31.6
	256	75.4	66.4	82.3	59.6	72.0	91.2	51.5	62.1	56.7	31.5
Zr-Shot		75.6	53.1	82.7	60.4	76.1	91.1	51.5	61.2	58.0	31.3

Table 24. Ablation study over the effect of the number of attention heads used by LoRSU to fine-tune the image encoder. We report the VQA accuracies of the last session in the *50-shot* CL setting. The accuracies on the target dataset are in red color. For this experiment, we use $r = 64$ for the rank of LoRSU.

		VQA Datasets (Acc %)									
FT Dataset	# heads	GTS	TSI	CAn	AIR	ESAT	DALLE	VSR	HM	MMVP	VisOnly
GTS	0	83.1	52.7	82.2	60.8	60.6	91.1	51.6	61.7	59.3	31.6
	1	83.9	53.8	82.0	60.7	55.4	91.2	51.6	61.6	60.0	31.8
	2	84.9	53.2	81.3	60.7	61.7	90.9	51.5	61.9	59.3	31.3
	4	84.7	53.5	81.0	60.5	60.5	90.6	51.5	61.8	58.7	31.5
	8	84.9	52.9	81.2	60.5	58.8	90.5	51.5	61.6	59.3	31.5
	16	85.0	53.1	81.3	60.0	59.2	90.6	51.5	61.6	56.7	31.3
TSI	0	75.1	64.2	82.1	59.3	72.2	90.8	51.5	61.8	57.3	31.5
	1	75.3	64.8	81.9	59.5	74.0	90.5	51.5	61.6	58.0	32.0
	2	75.3	72.1	82.0	59.3	72.3	90.5	51.6	61.4	58.0	31.6
	4	74.9	66.8	82.2	58.9	74.0	90.5	51.5	62.1	58.0	31.4
	8	74.7	67.4	81.7	59.1	71.5	91.2	51.5	62.2	58.0	31.7
	16	75.3	65.2	81.8	59.9	69.1	90.5	51.5	61.6	58.0	31.3
Zr-Shot		75.6	53.1	82.7	60.4	76.1	91.1	51.5	61.2	58.0	31.3

Table 25. Robustness comparison of LoRSU with respect to the number of training epochs. We consider LoRSU, *LoRSU-Rand* where the k attention heads are chosen randomly and *LoRSU-AAH* where all the attention heads are chosen for fine tuning. We use *50 shots* on the *GTS* for each method and we report the Target Improvement (*TI*) on this dataset and the Control Change (*CC*) using only ESAT as a control dataset. We include error bars over 3 runs.

# Epochs	LoRSU-Rand		LoRSU-AAH		LoRSU	
	TI (\uparrow)	CC (\uparrow)	TI (\uparrow)	CC (\uparrow)	TI (\uparrow)	CC (\uparrow)
2	5.2 \pm 0.9	-11.1 \pm 1.1	6.1 \pm 0.3	-11.6 \pm 0.7	5.6 \pm 0.4	-9.7 \pm 0.8
5	7.6 \pm 0.8	-15.0 \pm 0.9	9.3 \pm 0.4	-15.6 \pm 0.6	8.6 \pm 0.3	-12.6 \pm 0.5
10	7.8 \pm 0.5	-18.1 \pm 0.8	9.1 \pm 0.1	-19.6 \pm 0.5	9.7 \pm 0.1	-14.3 \pm 0.7
20	5.9 \pm 0.6	-20.0 \pm 0.7	8.1 \pm 0.1	-21.5 \pm 0.6	7.4 \pm 0.2	-15.7 \pm 0.6



Figure 4. Instances of the ‘Use Laptop’ action.

F. TSI vs. DALLE

In Figures 4 through 7, we present examples of images from TSI and DALLE for different actions. In general, we observe that TSI comprised of natural, unposed images of senior individuals performing daily tasks, reflecting real-life scenarios. The images are broader, showing the surrounding environment, which is crucial for context. On the other hand, DALLE images are idealized or stylized images. The focus is narrower, with emphasis on the object of the action (e.g. tablet, glass, etc.).

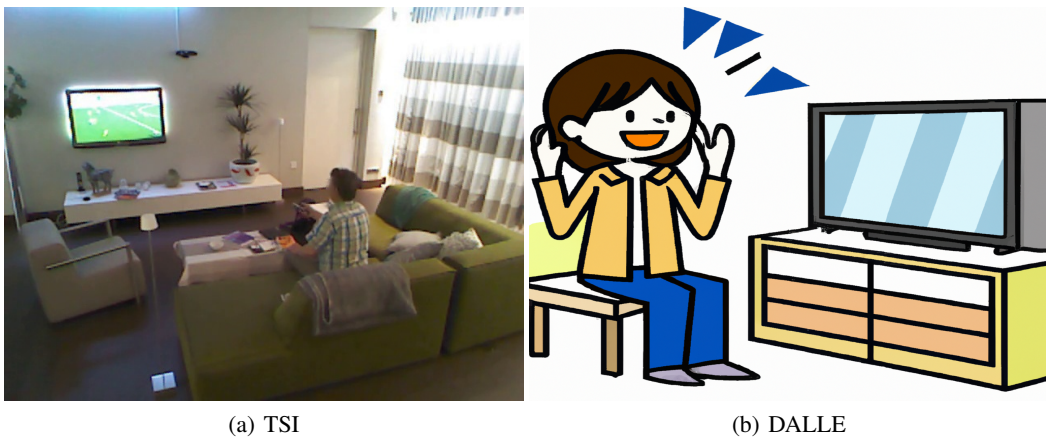


Figure 5. Instances of the ‘Watching TV’ action.

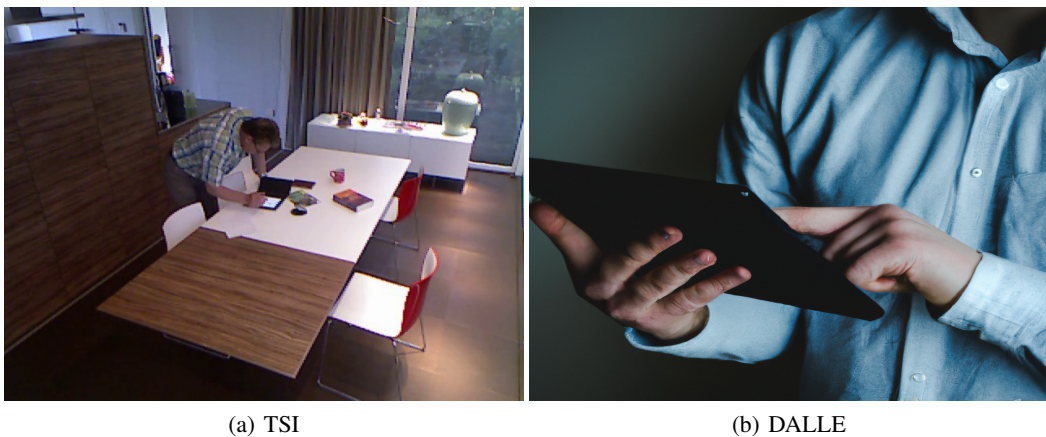


Figure 6. Instances of the ‘Use Tablet’ action.



Figure 7. Instances of the ‘Use a telephone’ action.